Neoplasia 68 (2025) 101220

Contents lists available at ScienceDirect

Neoplasia

journal homepage: www.elsevier.com/locate/neo

Original Research

Neuropilin-2 upregulation by stromal TGFβ1 induces lung disseminated tumor cells dormancy escape and promotes metastasis outgrowth

L Recalde-Percaz [a,b], I de la Guia-Lopez [c,d,1], P Linzoain-Agos [c,d,1], A Noguera-Castells [a,b,2], M Rodrigo-Faus [c,d,2], P Jauregui [a], A Lopez-Plana [a,b], P Fernández-Nogueira [a,b,e], M Iniesta-González [c,d], M Cueto-Remacha [c,d], S Manzano [c,d,f], R Alonso [a], N Moragas [a,b], C Baquero [c,d], N Palao [c,d], E Dalla [g], FX Avilés-Jurado [h,i,j], I Vilaseca [h,i,j], X León-Vintró [k,l], M Camacho [m], G Fuster [a,b,n], J Alcaraz [e,o], J Aguirre-Ghiso [g,p], P Gascón [a,b], A Porras [c,d], A Gutiérrez-Uzquiza [c,d], N Carbó [b], P Bragado [c,d,*]

[a] Department of Biomedicine, School of Medicine, Universitat de Barcelona, 08036 Barcelona, Spain
[b] Department of Biochemistry and Molecular Biomedicine, Faculty of Biology, Institute of Biomedicine (IBUB), Universitat de Barcelona, 08028 Barcelona, Spain
[c] Department of Biochemistry and Molecular Biology, Faculty of Pharmacy, Complutense University of Madrid, 28040 Madrid, Spain
[d] Health Research Institute of the Hospital Clínico San Carlos, 28040 Madrid, Spain
[e] Unit of Biophysics and Bioengineering, Department of Biomedicine, School of Medicine and Health Sciences, Universitat de Barcelona, Barcelona, Spain
[f] Instituto de Investigación Sanitaria (IIS) Biodonostia, 20014 San Sebastián/Donosti, Spain
[g] Department of Cell Biology, Cancer Dormancy and Tumor Microenvironment Institute, Albert Einstein Cancer Center, Albert Einstein College of Medicine, New York, NY, USA
[h] Functional Unit of Head and Neck Tumors. Otorhinolaryngology Head-Neck Surgery Department, Hospital Clínic, Barcelona, Spain
[i] Translational Genomics and Target Therapies in Solid Tumors Group. Institut dInvestigacions Biomèdiques August Pi i Sunyer. IDIBAPS, Barcelona, Spain
[j] Surgery and Medical-Surgical Specialties Department. Faculty of Medicine and Health Sciences. Universitat de Barcelona. Barcelona, Spain
[k] Otorhinolaryngology Department, Hospital de la Santa Creu i Sant Pau, Universitat Autònoma de Barcelona, 08193 Barcelona, Spain
[l] Centro de Investigación Biomédica en Red de Bioingeniería, Biomateriales y Nanomedicina (CIBER-BBN), 28001 Madrid, Spain
[m] Genomics of Complex Diseases, Research Institute Hospital Sant Pau, IIB Sant Pau, 08041 Barcelona, Spain
[n] Department of Biosciences, Faculty of Sciences and Technology, University of Vic, 08500 Vic, Spain
[o] Institute for Bioengineering of Catalonia (IBEC), The Barcelona Institute for Science and Technology (BIST), Barcelona 08028, Spain
[p] Gruss-Lipper Biophotonics Center, Ruth L. and David S. Gottesman Institute for Stem Cell Research and Regenerative Medicine Albert Einstein Cancer Center, Albert Einstein College of Medicine, New York, NY, USA

ARTICLE INFO

Key words:
Neuropilins
dormancy
disseminated tumor cells
TGFβ
metastasis
breast cancer
head and neck cancer

ABSTRACT

Metastasis is the main cause of death from solid tumors. Therefore, identifying the mechanisms that govern metastatic growth poses a major biomedical challenge. Tumor microenvironment signals regulate the fate and survival of disseminated tumor cells (DTCs) in secondary organs. However, very little is known about the role of nervous system mediators in this process. We have previously reported that neuropilin-2 (NRP2) expression in breast cancer correlates with poor prognosis. Here, we show that NRP2 positively regulates the proliferation, invasion, and survival of breast and head and neck cancer cells *in vitro*. NRP2 deletion in tumor cells inhibits tumor growth *in vivo* and decreases the number and size of lung metastases by promoting lung DTCs quiescence. NRP2 deletion upregulates dormancy and cell cycle regulators expression and promotes DTCs reprograming into quiescence. Moreover, lung fibroblasts and macrophages induce NRP2 upregulation in DTCs through the secretion of TGFβ1. NRP2 facilitates lung DTC interaction with the extracellular matrix and promotes lung DTCs activation and metastasis. Therefore, we conclude that the TGFβ1-NRP2 axis is a new key dormancy-awakening inducer that promotes DTCs proliferation and lung metastasis development.

* Corresponding author.
E-mail address: pbragado@ucm.es (P. Bragado).
[1] These authors have contributed equally.
[2] These authors have contributed equally.

https://doi.org/10.1016/j.neo.2025.101220
Received 6 February 2025; Received in revised form 11 August 2025; Accepted 12 August 2025
Available online 22 August 2025
1476-5586/© 2025 The Authors. Published by Elsevier Inc. This is an open access article under the CC BY-NC-ND license (http://creativecommons.org/licenses/by-nc-nd/4.0/).

INTRODUCTION

Metastasis is the dissemination of tumor cells to a secondary organ, where a macroscopic secondary tumor grows. It is the main cause of death associated with solid tumors, as more than 90% of patients die from metastatic disease [1]],[. Metastasis is considered the last of a complex and dynamic cascade of steps in which tumor cells grow, escape from the primary tumor (PT), migrate, intravasate, disseminate via the circulatory system, colonize secondary organs, enter dormancy, survive, and reinitiate growth to form secondary tumors [1,2]. Metastases are derived from disseminated tumor cells (DTCs) that escape from the primary tumor (PT) and invade secondary organs where they proliferate, generating a secondary tumor bulk [2,3]. However, metastases can appear months or years after PT diagnosis and treatment because of the clinically occult state that DTCs acquire, known as dormancy, in which they become quiescent and resistant to antiproliferative therapies [3,4]. Dormancy is a reversible cell cycle arrest from which DTCs can escape through mechanisms that remain unclear [2].

According to the seed and soil theory [5,6], the tumor microenvironment (TME) exerts a regulatory effect on the biology of metastases and DTCs, tightly controlling metastasis. Consistent with this, we previously showed that in head and neck squamous cell carcinoma (HNSCC) models, TGFβ2 regulates DTCs quiescence in the bone marrow (BM) through binding to TGFβR3 [7]. Likewise, other studies have reported additional TME regulators of DTCs fate, such as TSP-1 [8], Gas6 [9] or BMP7 [10]. However, the mechanisms that control DTCs dormancy, reactivation, and proliferation are still not well understood.

In recent years, the contribution of nerves and neural derived factors to the regulation of tumor progression has emerged as an important component of the TME [11,12]. Two pioneering studies in prostate [13] and gastric cancer [14] showed that nerves are an essential component of the TME and that neoneurogenesis plays a key role in cancer progression and metastasis. More recently, it has been shown that remodeling of the extracellular matrix by Schwann cells potentiates metastasis initiation [15]. Furthermore, it also has been reported that the sympathetic nervous system is also implicated in the reactivation of dormant DTCs in the BM niche [16]. Using bioinformatic tools and patient databases, we have identified several neuronal-related genes that are differentially expressed among breast cancer (BrCa) subtypes [17], suggesting that neural-related factors are implicated in BrCa initiation and progression. Neuropilin-2 (NRP2) appears to be overexpressed in the basal-like BrCa subtype [17], the most aggressive BrCa subtype that usually presents with low dormancy periods and develops metastasis in the first 5 years after diagnosis. Furthermore, high NRP2 expression in triple negative BrCa patients correlates with worse prognosis [17]. Similarly, in HNSCC, transcriptional expression of Semaphorin-3F and NRP-2 correlates with a higher risk of occult nodal metastases [18]. NRPs are multifunctional proteins that act as co-receptors for class 3 semaphorins (SEMA3s) and diverse growth factors such as vascular endothelial growth factors (VEGF) and TGFβ1 [19]. NRPs expression is commonly aberrant in tumors; thus, it can modulate multiple tumorigenic processes [20]. How DTCs interact with neural-derived cues present in the microenvironment to regulate dormancy and survival at metastatic sites is largely unknown. In this study, we defined the role of NRP2 in lung DTCs regulation and progression into metastasis in preclinical models of BrCa and HNSCC.

MATERIALS AND METHODS

The data generated in this study are available within the article and its supplementary data files, and raw data are available upon request from the corresponding author.

Cells lines and cultures

Human BrCa cell lines were obtained from the American Type Culture Collection (ATCC; Rockville, MD) and grown in DMEM, DMEM/F12 or RPMI-1640 media at 37°C and 5% CO_2 according to the ATCC indications for each cell line. The media were supplemented with 10% fetal bovine serum (FBS), 5% Glutamax, and 5% penicillin-streptomycin (Gibco), hereafter referred to as complete culture media. In the case of BT-549 and BT-474 cell lines, the media were supplemented with 10 μg/mL human insulin (Sigma-Aldrich). MDA-MB-453-PT and MDA-MB-453-Lu cells were obtained and cultured as previously described [21].

HNSCC cell lines were generated as described previously [7] and grown in DMEM/F12 complete media at 37°C and 5% CO_2. HEp3 cells were maintained as primary cultures and cultured *in vitro* until passage four. They were maintained *in vivo* using the chicken embryo chorioallantoic membrane (CAM) model [22] or nude mice.

Human lung fibroblast CCD-19 cells were kindly donated by Dr. Alcaraz (University of Barcelona, Spain) and cultured in DMEM/F12 complete media at 37°C and 5% CO_2. The human monocyte cell line THP-1 was kindly donated by Dr. Julve (University of Barcelona, Spain). THP-1 cells were cultured at 37°C and 5% CO_2 according to ATCC indications. They were differentiated into monocyte-derived macrophages using 50 ng/mL 12-O-tetradecanoylphorbol-l3-acetate (PMA; Sigma-Aldrich) for 4 days. Total differentiation of monocyte-derived macrophages was achieved by removing the PMA-containing media and incubating the cells in fresh culture media for 1-2 days.

CRISPR/Cas9

To efficiently delete NRP2, CRISPR-Cas9 technology using the double lentiviral system designed by Zhang laboratory was used [23]. First, Cas9-expressing T-HEp3 and MDA-MB-231 cells were generated. Briefly, LentiCas9-Blast lentiviral particles were generated in HEK293T cells transforming them with DNA-Lipofectamine lipid complexes. Lipofectamine 3000 transfection reagent (#15292465, Invitrogen) was mixed with a mixture of the packaging (psPAX2; #12260, Addgene), enveloping (pMD2-VSVg; #12259, Addgene) and LentiCas9-Blast (#52962, Addgene) plasmids in Opti-MEM medium (#31985-070, Gibco) in a 1:1 ratio. Next day, media was changed and replaced with fresh complete media. After 72h, the media was collected, centrifugated at 500g for 5min and filtered with 0.45μm PES filter (#4654, Pall Life Science). T-HEp3 and MDA-MB-231 parental cells were transduced with the lentiviral-enriched supernatant, and cells were incubated at 37°C and 5% CO_2. After 24h, media was changed and 48h later, blasticidin selection (10μg/mL) was performed. Individual clones were expanded and Cas9 presence was verified by western blot.

Second, specific NRP2 guide RNAs (gRNA) were annealed and cloned in lentiGuide-puro plasmid (#52963, Addgene) using BsmBI cloning site (5'-CACCGGACTGCAAGTACGATTGGC-3' (forward) and 5'-AAACGCCAATCGTACTTGCAGTCC-3' (reverse)). Viral productions to deliver gRNA in cells were performed as previously described using packaging, enveloping and plentiGuide (LG)-puro plasmids containing gRNAs against NRP2 (LG-NRP2) or non-targeting (NTC) sequence (5′-CACCGCGGCTGAGGCACCTGGTTTA-3′ (forward) and 5'-AAACTAAACCAGGTGCCTCAGCCGC-3′ (reverse)).

Finally, Cas9 positive T-HEp3 and MDA-MB-231 cells were transduced with LG-NRP2 or LG-NTC lentivirus containing media, diluted 1:4 in fresh antibiotic free complete media. After 24h, media was changed and 48h later, blasticidin (10μg/mL) and puromycin (1μg/mL) selection was performed. Individual clones were expanded and NRP2 deletion was verified by genomic DNA sequencing (**table S1**), qPCR and western blot.

In vivo mice models

All animal experiments were performed in accordance with the regulations of our institution's ethics commission, following the guidelines established by regional authorities (Catalonia, Spain). Five-week-old female NOD-SCID mice (CB17/IcrHanHsd-PrKdc Scid) were

obtained from Janvier Labs (France, Europe) and maintained under specific-pathogen free (SPF) health conditions at a constant ambient temperature (22–24°C) and humidity (30–50%). The MMTV–Her2 immune-competent transgenic mice were bred in and obtained from Aguirre-Ghiso's laboratory at Mount Sinai School of Medicine, USA. 14 to 18-weeks-old female mice were used as early ('pre-malignant') stage and 20-weeks-old female mice with palpable tumor(s) were used as late stage of cancer progression [24]. For the fibrosis experiments, we used Rapgef1$^{Flox/Flox}$; PF4-Cre$^{-/-}$ mice that were bred and obtained from Dr. Porras' laboratory at Complutense University, Spain. Young (6-weeks mice) 'mice' and old (16-month-old) months mice were used.

Xenograft tumors were obtained by orthotopic inoculation of a 1:1 ratio mixture of Matrigel and PBS++ (supplemented with 1mM $MgCl_2$ and 0.5mM $CaCl_2$), in a final volume of 100μL per mouse. Either 8×10^5 T-HEp3-NTC or T-HEp3-NRP2^{KO} cells were inoculated into the neck area (5 mice per condition). 10^6 MDA-MB-453 cells were inoculated into the mammary gland. Mouse weight and tumor size were measured twice per week using a caliper, and tumor volume (V) was calculated as $V=(D \times d)^2/2$ (D: long diameter; d: short diameter). In the MDA-MB-453 model, the mice were euthanized after 3 months. For the T-HEp3 model, once the mean tumor volume was over 500mm^3, PTs were surgically removed, and the mice were left for an additional 4 weeks. Surgically removed PTs were measured, weighed, and stored at -80°C for protein and RNA extraction, or fixed in 4% paraformaldehyde (PFA) for further immunohistochemical analyses. After four weeks of growth, the mice were anesthetized and euthanized in accordance with the regulations of the institution's ethics commission. At the end point, potential metastatic organs, such as the lungs, were surgically removed and fixed in 4% PFA for the analysis of the presence of DTCs.

For the lung metastasis *in vivo* experiments, 2.5×10^5 wild-type T-HEp3, T-HEp3-NTC, or T-HEp3-NRP2^{KO} cells or 5×10^5 MDA-MB-231-Cas9 or MDA-MB-231-NRP2^{KO} cells were inoculated in a final volume of 100μL in PBS++ into the lateral caudal tail vein (5 mice per group). The weight of the mice was measured twice per week. Two and four weeks after inoculation, the mice were anesthetized and euthanized in accordance with the regulations of the institution's ethics commission. At the end point, the lungs were removed for metastasis assessment by fixing them in 4% PFA for analysis of the presence of DTCs by immunocytochemistry.

Quantification and outcome assessment of the *in vivo* studies were performed in a blinded fashion.

Studies with patients

NRP2 mRNA expression was analyzed using BrCa patient data from the GOBO [25] and Kaplan-Meier plotter [26] public databases. Additionally, in collaboration with Dra. Camacho and Dr. Leon from Sant Pau Hospital (Barcelona, Spain) *NRP2* mRNA expression was analyzed by RT-qPCR in PT samples from a cohort of 92 HNSCC patients and correlated it with distant metastasis-free survival (DMFS). Publicly available RNA-seq data from breast cancer cohort (BRCA) head and neck cancer (HNSC) was downloaded from TCGA database. For both cohorts, tumor patient samples were divided by the median NRP2 expression. R statistical environment v.4.5.1 [27] and DESeq2 v.1.48.1 [28] were used to investigate the differential expressed genes between patients expressing high and low levels of NRP2.

3D Cultures

To analyse the functional characteristics and the phenotypic features of the tumour cells on-top 3D cultures in BD Matrigel™ Basement Membrane Matrix were performed in 8-well chamber slides (#354108, BD Falcon CultureSlide). Briefly, $1{\cdot}10^3$ MDA-MB-231 or T-HEp3 cells per well were seeded in 400μL of 3D culture media (DMEM-F12 + 5% FBS + 1% Penicillin-Streptomycin + 2% matrigel) on a matrigel layer. Cells were cultured for 7 days and media was changed every 3-4 days, while treating every two days with TGFβ1 (2ng/mL) by adding it directly to the well.

For 3D experiments fixation, media was carefully aspirated and cells fixed by RT incubation with 4% PFA for 20min. Finally, the slides were washed and stored at 4°C with PBS until further analysis.

In vivo chicken embryo model

The chicken chorioallantoic membrane (CAM) model was previously described [7,22]. Briefly, we used premium specific pathogen-free (SPF), fertile, 11-day-incubated embryonated chicken eggs supplied by Gibert farmers (Tarragona, Spain). $3{\cdot}10^5$ Lu-HEp3 cells (diluted in PBS++) were inoculated per egg and tumours were grown for 6 days. When specified, the tumours were treated with αNRP2 (10ng/mL daily) for 5 days. On day 6 after inoculation, the tumours were excised, weighed, measured and immediately fixed in 4% PFA to perform IF analysis. Additionally, chicken embryos lungs were also isolated for cell dissemination analysis.

Generation of conditioned media

For experiments with conditioned media (CM), cell lines were cultured up to 80% confluence and maintained in serum-free media for 48h. Their culture media was collected, filtered with 0.22μm filters and centrifuged (1200rpm, 5min) to discard unattached cells and cell debris. For lung CM generation, lung tissues from healthy animals were dissected and dissociated by incubation with 200U/mL collagenase type IV and 100U/mL bovine serum albumin (BSA) solution (#C9891, Sigma-Aldrich) for 30min at 37°C. The tissue cell suspension was homogenized, centrifuged and the cell pellet was resuspended in DMEM/F12 complete media. After 24h, fresh cell media was added and when 80% confluence was obtained, lung CM was generated as previously described [7].

Immunoprecipitation assay

To deplete TGFβ1 from CM, 10mg/mL magnetic beads (#10003, Invitrogen) were incubated with 10μg anti-TGFβ1 antibody (#sc-52893, Santa Cruz) or matched IgG isotype control (#31903, Invitrogen) in serum-free media. The beads-antibody solution was pre-incubated during 1h at 4°C and rotation movement. The magnetics beads were isolated using the magnetic rack and 1mL of the CM was added and incubated overnight (ON) at 4°C with rotation movement. The next day, centrifugation and isolation of magnetic beads was performed using the magnetic rack and the supernatant was collected for its immediate use for cell treatment.

RNA-Seq data processing and analysis

Total RNA was extracted from T-HEp3 NTC cells and T-HEp3 NRP2^{KO} cells cultured for 24 h. RNA sequencing was performed and analyzed by the genomic CAI at Complutense University using the Illumina NovaSeq 6000 platform. RNA-Seq data was analysed using the commercial CLC Genomics Workbench (Qiagen) available at the genomic CAI. The steps for the analysis were a first filtering of quality and possible adapters in the readings, and then they are launched into the RNASeq analysis of each sample and then the differential expression comparisons. Lowly expressed genes were filtered out when accounting for less than 15 read counts across all samples

Principal component and differential gene expression analysis

Unsupervised analysis was performed by principal component analysis (PCA) using Reads Per Kilobase Million (RPKM) values to determine sample variance. Then, differential expression analysis was carried out using DESeq2 v1.34.0 [28] with the design formula ~ Condition, a factor with two different levels (KO-CTL). Genes were

considered differentially expressed (DEG) using a 5% FDR and an absolute log2 Fold Change ≥1.5 as thresholds. DEGs were visualized using a heatmap, with gene expression values scaled by z-score. Samples and genes were clustered using Euclidean distance and the ward.D2 linkage method.

Gene ontology overrepresentation analyses

Gene ontology (GO) overrepresentation analysis of biological process terms was performed using the clusterProfiler v4.4.2 [29] and org.Hs.eg.db v3.14.0 [30]. Redundant GO terms were excluded for graphical representation using the rrvgo v1.6.0 [31], that is based in semantic similarity and adjusted p-value. The most significantly enriched pathways were represented using ggplot2 v3.5.2 [32].

Gene set enrichment analysis

Gene set enrichment analysis was performed using EnrichR. Briefly, differentially expressed genes were used altogether with Gene Ontology databases (Biological Processes, Cellular Components and Molecular Function), Human Phenotype Ontology and Hallmark, Oncogenic Signatures from Molecular Signature Databases (MSigDB). A gene set was considered enriched using a 5% FDR. Gene set enrichment analyses were performed using GSEA v.4.3.3 [33]

Adhesion assays

100,000 cells per well were seeded in 12-well plates in culture medium with 10% FBS on 3 different matrices: plastic, type I collagen (11179179001) and matrigel (356231), and incubated at 37°C and 5% CO_2 for 30 minutes. After that time, the cells were fixed by washing with PBS 1X and incubating with 2% ethanol violet crystal at room temperature for 20 minutes. Finally, photos of 5 representative fields for each condition were taken with the NIS-ElementsF 2.20 program using the Nikon Eclipse TE300 microscope.

Statistical analysis

The results were graphically plotted and statistically analyzed using GraphPad Prism7 software. Graphs represent the mean value of the samples ± the standard error of the mean (S.E.M.). To compare two experimental groups, the unpaired *t*-Student's t-test was used, whereas one-way ANOVA or two-way ANOVA tests were used to compare more than two groups, with one or two variables, respectively. Multiple comparison tests were also conducted. Statistical significance was considered when the p-value was < 0.05, following the next annotation: * $p \leq 0.05$, ** $p \leq 0.01$, *** $p \leq 0.001$, and **** $p \leq 0.0001$.

RESULTS

NRP2 Promotes proliferation and cell cycle progression concomitantly with downregulation of dormancy and cell cycle regulators

To determine the role of NRP2 in dormancy regulation, we first assessed the expression of NRPs in a panel of BrCa cells previously characterized as either proliferative/low-dormancy score (LDS) or dormant-like/high-dormancy score (HDS) cells [34] based on the ratio between the expression of positive dormancy genes and negative dormancy genes. MDA-MB-231, MDA-MB-468, HCC1954, and BT-549 were identified as LDS cell lines and BT-474, T-47D, MDA-MB-453, and ZR-75-1 as HDS cells [34]. We observed that *NRP1* and *NRP2* mRNA were upregulated in LDS cell lines compared to HDS cells, whereas *NRP2* gene expression was downregulated in HDS cells compared to that in non-malignant mammary epithelial MCF10A cells (Fig. 1A). Consistently, NRP2 protein expression was upregulated in LDS cells, particularly in MDA-MB-231 and BT-549 cells, whereas it was poorly expressed in the HDS cell lines (Fig. 1B). We also examined the expression of NRPs in a panel of HNSCC cell lines with a known proliferative or dormant phenotype previously generated from lung (Lu) or bone marrow (BM) DTCs using an HNSCC patient-derived xenograft (PDX) model (T-HEp3) [7]. Lung DTC-derived cell line (Lu-HEp3) exhibits proliferative/LDS, whereas the BM DTC-derived cell line (BM-HEp3) exhibits a quiescent/dormant/HDS phenotype [7]. In addition, we used an *in vitro* derived dormant variant of HEp3 (D-HEp3) [7,35]. Analysis of NRPs mRNA and protein expression in HNSCC cells confirmed that NRP2 was upregulated in proliferative/LDS cells, not only in the parental cell line but also in the cell line derived from Lung DTCs (Fig. 1C, D). NRP1 expression was also downregulated in BrCa and HNSCC HDS cell lines (**fig. S 1A-B)**. However, Lu-Hep3 cells expressed very low levels of NRP1 at both the mRNA and protein levels (**fig. S1C-D).** These results revealed that NRP2 expression is downregulated in both BrCa and HNSCC dormant cell lines, whereas its expression correlates with a more proliferative phenotype and is upregulated in the lung DTC-derived cell line.

Prompted by our observed inverse correlation between NRP2 expression and quiescence, we sought to characterize NRP2 role in cell proliferation by generating stable NRP2-knockouts ($NRP2^{KO}$) in LDS cell lines from BrCa and HNSCC using CRISPR-Cas9 (Fig. 1E **and fig. S1E-I and table S1**). We first analyzed NRP2 role in tumor cell proliferation and found that $NRP2^{KO}$ cells proliferated more slowly than control cells in both MDA-MB-231 (Fig. 1F) and T-HEp3 cell lines (Fig. 1G). Moreover, deletion of NRP2 decreases the expression of the proliferation marker, Ki67, both in T-HEp3 and MDA-MB-231 cells (**fig. S2A-B**). Furthermore, we found that NRP2 deletion induced cell cycle arrest (Fig. 1H-I). MDA-MB-231 $NRP2^{KO}$ cells were arrested in the G2/M phase (Fig. 1H), whereas T-HEp3 $NRP2^{KO}$ cells were arrested in G1 (Fig. 1I). Cell cycle progression relies on protein complexes composed of cyclins and cyclin-dependent kinases (CDKs). To prevent abnormal proliferation, nuclear Cip/Kip proteins such as p21 and p27 act as catalytic inhibitors of CDKs [36]. Analysis of p27 expression showed that NRP2 expression modulation notably increased p27 protein levels (Fig. 1E). In addition, deletion of NRP2 also increases the expression of p21 (**fig. S2C-D**). In agreement with this, deletion of NRP2 induces upregulation of other cyclin dependent kinase inhibitors such as *CDKN2A* (p15) and *CDKN2B* (p16) and several dormancy regulators such as *TGFBR3, NR2F1, SOX9, RARB and DEC2* [7,37] (Fig. 1J-K). However, no differences were observed in the levels of phosphorylated (active) p38 Mitogen activated protein Kinase (MAPK) and extracellular signal-regulated kinase (ERK) and the p-ERK/p-p38 ratio [7,38] (**fig. S2E-F**), suggesting that other factors altered upon NRP2 loss may be required to elicit a full dormant phenotype. Collectively, these results indicated that NRP2 is a pro-tumorigenic and/or anti-dormancy protein that induces tumor cells proliferation while inhibiting cell cycle arrest, probably by altering cyclin dependent kinase inhibitors, such as p27, expression.

NRP2 Deletion inhibits tumor-initiation capacity in vitro and blocks tumor growth in vivo

To test whether NRP2 could also regulate tumor initiation capacity, we performed anchorage-dependent colony formation assays and observed that NRP2 deletion decreased the number of foci formed by MDA-MB-231 cells (Fig. 2A) and T-HEp3 cells (Fig. 2B), revealing the tumor initiation capacity enhancement of NRP2 in BrCa and HNSCC cells.

We then analyzed the specific contribution of NRP2 to tumor growth *in vivo* by orthotopically inoculating NRP2 knockout and control T-HEp3 cells. When PTs reached volumes $> 500mm^3$, they were surgically removed (Fig. 2C). NRP2 depletion strongly suppressed tumor growth *in vivo*, whereas control tumors derived from NTC cells grew rapidly. Control tumors had to be surgically removed 16 days after inoculation (Fig. 2D). Interestingly, $NRP2^{KO}$ cell-derived tumors showed a delay of 1

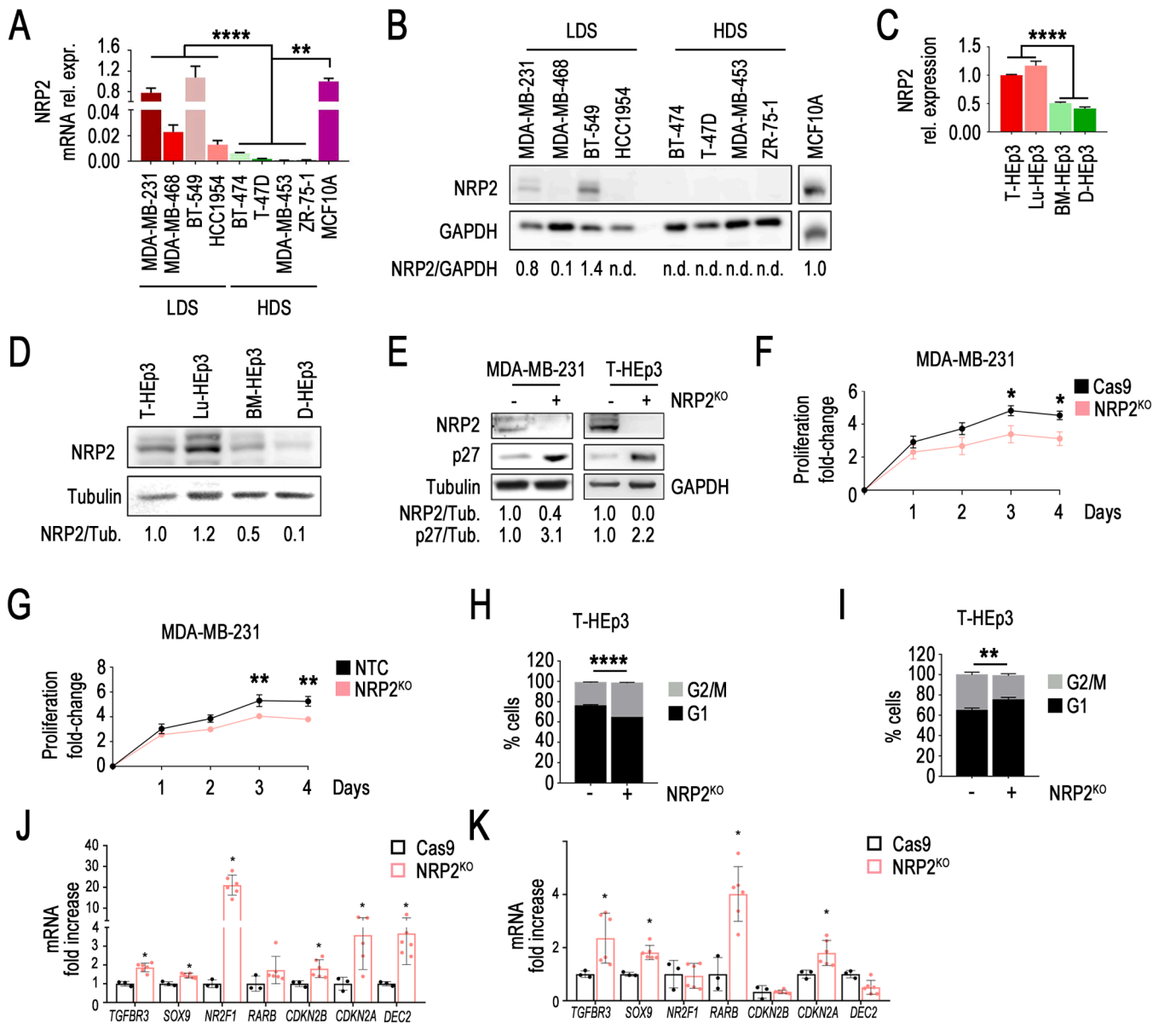


Fig. 1. NRP2 deletion in proliferative cells alters cell cycle and decreases cell proliferation, by inducing p27 expression. A) Analysis of *NRP2* mRNA relative expression in human healthy mammary epithelial (MCF10A) and BrCa cell lines. The bar plot shows relative quantification (RQ) values referred to MCF10A cells (n=3). The graph represents RQ mean values ± S.E.M.; **P < 0.01, ****P < 0.0001 comparing LDS (MDA-MB-231, MDA-MB-468, HCC1954, BT-549) *vs* HDS (BT-474, T-47D, MDA-MB-453, ZR-75-1) cell lines by *t*-Student's test. **B)** Representative western blot analysis of NRP2 protein levels normalized with GAPDH. Protein quantifications are referred to MCF10A. n.d.=non detectable. (n=3). **C)** Analysis of *NRP2* mRNA relative expression in HNSCC cell lines. The bar plot shows RQ mean values ± S.E.M. referred to T-HEp3 cells (n=3); ****P < 0.0001 comparing proliferative/LDS (T-HEp3, Lu-HEp3) *vs* dormant/HDS (BM-HEp3, D-HEp3) cell lines by *t*-Student's test. **D)** Representative western blot analysis of NRP2 protein levels normalized with α-tubulin. Protein quantifications are referred to T-HEp3 cells (n=3). **E)** Representative western blot analysis of NRP2 and p27 protein levels normalized with α-tubulin in NRP2^{KO} cells (n=3). NRP2 and p27 quantifications are referred to the non-target control. **F-G)** MDA-MB-231 (**F**) and T-HEp3 (**G**) cells proliferation in control (Cas9, NTC) *vs NRP2*-deleted cells (NRP2^{KO}). Graphs represent the fold-change of proliferation mean ± S.E.M. referred to day 0 (n=2); *P < 0.05, **P < 0.01 comparing Cas9/NTC *vs* NRP2^{KO} by one-way ANOVA, Sidak's test. **H-I)** Percentage (%) of MDA-MB-231 (**H**) and T-HEp3 cells (*I*) in each cell cycle's phase in control (-) and *NRP2*-deleted (NRP2^{KO}) cells (+). The bar plots represent mean ± S.E.M. (n≥2); **P < 0.01, ****P < 0.0001 comparing Cas9/NTC (non-targeted cells) *vs* NRP2^{KO} by two-way ANOVA, Sidak's test. J-K) Analysis of *TFGBR3, SOX9, NR2F1, RARB, CDKN2A, CDKN2B and DEC2* mRNA relative expression in MDA-MB-231 (J) and T-HEp3 (K) NTC and *NRP2*-deleted (NRP2^{KO}) cells after 24h. The bar plot shows relative quantification (RQ) values referred to the NTC cells (n=3). The graph represents RQ mean values ± S.E.M.; *P < 0.05 by *Mann Whitney* test.

month in growth compared to the control group, further supporting its role as a dormancy-regulatory protein (Fig. 2D). Moreover, NTC tumors were larger than NRP2^{KO} tumors in terms of PTs weight and volume (Fig. 2E), corroborating that NRP2 plays a key role in promoting tumor growth *in vivo*. NRP2 expression remained low in tumors bearing NRP2^{KO} cells (Fig. 2F) and, in agreement with the *in vitro* experiments, deletion of NRP2 also increased p27 and p21 levels and decrease Ki67 levels in tumor samples (Fig. 2G-I). Additionally, NRP2 depletion increased the expression of the apoptotic marker cleaved caspase 3 (cc3) in NRP2^{KO} cell-derived tumors (Fig. 2J), suggesting that NRP2 could also promote tumor cell survival. Taken together, these results suggest that NRP2 deletion reduces HNSCC tumor growth *in vivo* by promoting quiescence and apoptosis.

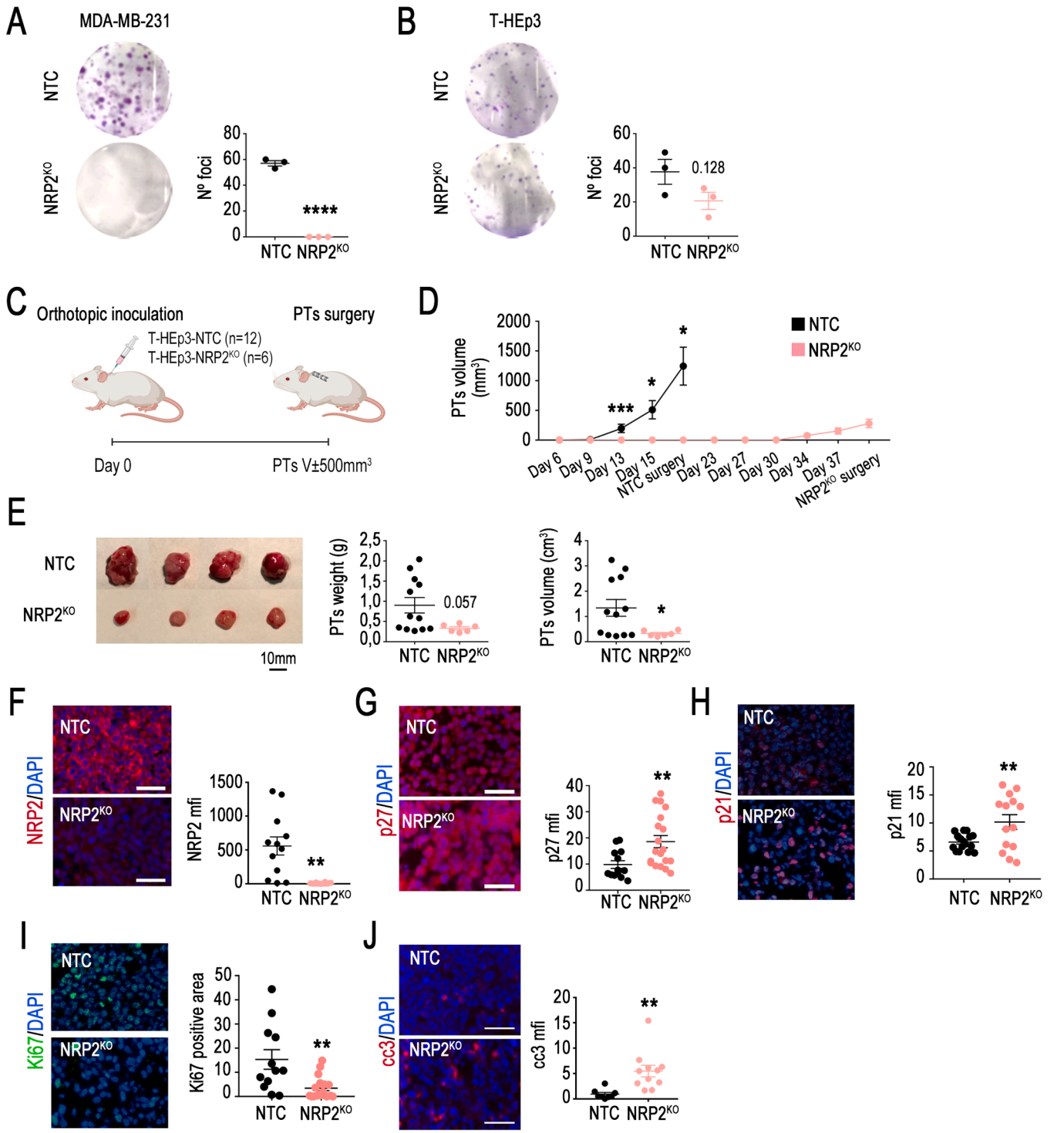


Fig. 2. NRP2 deletion inhibits T-HEp3 tumor growth. A, B) Left panels, representative images of colonies from anchorage-dependent growth assay in MDA-MB-231 (**A**) and T-HEp3 (**B**) cells. Right graphs, quantification of the total number of colonies. Graphs represent mean ± S.E.M. (n=1, triplicates); ns, non-significant, ****P < 0.0001, comparing non-target control (NTC) *vs* NRP2^{KO} by *t*-Student's test. **C)** Diagram of the orthotopic mice *in vivo* experiment using T-HEp3 control (NTC) *vs NRP2*-depleted (NRP2^{KO}) cells. **D)** Graph representing T-HEp3 tumors volume (mm^3) over time for each group. **E)** Left panel, representative T-HEp3 tumor images at the time of surgery. Middle and right panels, graphs showing PTs weight (g) (middle) and volume (cm^3) (right) at the time of surgery. **F-J)** Left panels, representative immunofluorescence (IF) images of NRP2 (**F**), p27 (**G**), p21 (**H**), Ki67 (**J**) and cc3 (**H**) in T-HEp3 mice tumors. Scale bar: 50μm. Right panels, mean fluorescence intensity (mfi) quantification of NRP2, p27, p21 and cc3. In Ki67 graphs the positive area for Ki67 staining was quantified. Graphs represent mean ± S.E.M. (n=1, with 12 mice for NTC and 6 mice for NRP2^{KO}); *P < 0.05, **P < 0.01, ***P < 0.001 comparing NTC *vs* NRP2^{KO} by *t*-Student's test.

NRP2 upregulation in lung DTCs drives lung micro-metastases emergence

Based on the link between NRP2 expression and cancer cell proliferation and tumor growth *in vitro* and *in vivo*, we characterized the role of NRP2 in migration and invasion *in vitro*. Wound-healing assays revealed that NRP2^{KO} MDA-MB-231 cells migrated less than Cas9 control cells (Fig. 3A), whereas NRP2 deletion in T-HEp3 cells had no effect on the cell migration capacity (**fig. S3**), suggesting that the NRP2 role in

regulating cell migration may be cell type-dependent. In contrast, the invasion capacity of the NRP2-depleted cells was significantly reduced compared to the control in both MDA-MB-231 (Fig. 3B) and T-HEp3 (Fig. 3C) cells, revealing that NRP2 promotes cancer cell invasion, which is a major step towards increased dissemination.

Our observation that NRP2 is upregulated in proliferative compared to dormant cell lines and that its deletion inhibits tumor growth and colony formation, through regulation of CDKs inhibitors and dormancy regulators, provides new insights into the role of NPR2 in the context of primary tumors. Next, we investigated whether NRP2 may also regulate the shift in DTCs between proliferation and quiescence in colonized organs. For this purpose, we first examined NRP2 expression in lung DTCs *in vivo* in xenograft models. We stained chicken and mouse lungs from control animals to detect T-HEp3 lung DTCs using vimentin-positive staining (Fig. 3D, top and middle panel). We also used the MMTV-Neu mouse model for BrCa, where multifocal breast carcinomas with lung metastases developed after 12-16 weeks of growth [39] to detect BrCa lung DTCs (by HER2 staining) (Fig. 3D, bottom panel). We found that vimentin in T-HEp3 DTCs and HER2 in BrCa DTCs were co-expressed with NRP2 (Fig. 3D), revealing that NRP2 is expressed in PT-derived lung DTCs. Moreover, in a lung metastasis *in vivo* experiment with wild-type T-HEp3 cells, we observed that the number of NRP2-positive cells was significantly higher in late lung macrometastases (isolated three weeks after inoculation) than in early lungs (isolated one week after inoculation) (Fig. 3E). Finally, to test whether NRP2 expression in lung DTCs could be regulated by the lung microenvironment, we inoculated MDA-MB-453 cells (low tumorigenic, HDS, and low expression of NRP2) orthotopically into the mammary fat pad of mice and allowed the tumors to grow for a long period (12 weeks) [21]. At the end point, the lungs were isolated, and cell dissemination was analyzed by detecting lung DTCs by HER2 staining. Surprisingly, we found that while single DTCs were still negative or expressed very low levels of NRP2 (Fig. 3F, upper panel), MDA-MB-453 DTC-derived lung micrometastases showed upregulated NRP2 (Fig. 3F, lower panel). These findings were validated in PTs and lung DTCs (Lu)-derived MDA-MB-453 primary cell line analysis, which showed increased NRP2 expression in the cell lines derived from lung DTCs (**fig. S4**). This suggests that upregulation of NRP2 optimizes DTCs conversion from a solitary cell state to proliferative clusters and metastasis outgrowth and supports the hypothesis that the lung microenvironment can upregulate NRP2 expression.

To investigate the role of NRP2 in lung DTCs, we used the lung DTCs primary cell line Lu-HEp3, which overexpresses NRP2 (Fig. 1D). Treatment of Lu-HEp3 cells with an NRP2 blocking antibody (αNRP2) *in vivo* had no effect on Lu-HEp3 PTs size (**fig. S5A**), although the levels of the proliferation marker Ki67 decreased in the tumors treated with the NRP2 blocking antibody *in vivo* (**fig. S5B**), suggesting that blocking NRP2 decreases Lu-HEp3 cells proliferation. In addition, blocking NRP2 activity increased the levels of the apoptotic marker cc3 in Lu-HEp3 tumors (**fig. S5C**), relating NRP2 to lung DTCs survival. These results highlight the key role of NRP2 in the regulation of lung DTCs' growth and survival.

Lung fibroblasts and macrophages-derived TGFβ1 induces DTCs NRP2 expression

We next explored the mechanisms that may support NRP2 upregulation in the lung microenvironment, which might favor metastasis. It has been reported that NRPs act as co-receptors of several soluble ligands and can be regulated by factors present in the TME [19,40,41], such as VEGF. We first treated the cells with VEGF-C, the main vasculogenic ligand of NRP2, to induce lymphatic endothelial cell proliferation and to promote cell migration and invasion [42]. Surprisingly, no differences were observed in NRP2 levels (**fig. S6A**). No effects were observed either when cells were treated with SEMA3F, the most important ligand of NRP2 that regulates axonal guidance in the nervous system [43] and tumor cell dissemination [44] (**fig. S6B**).

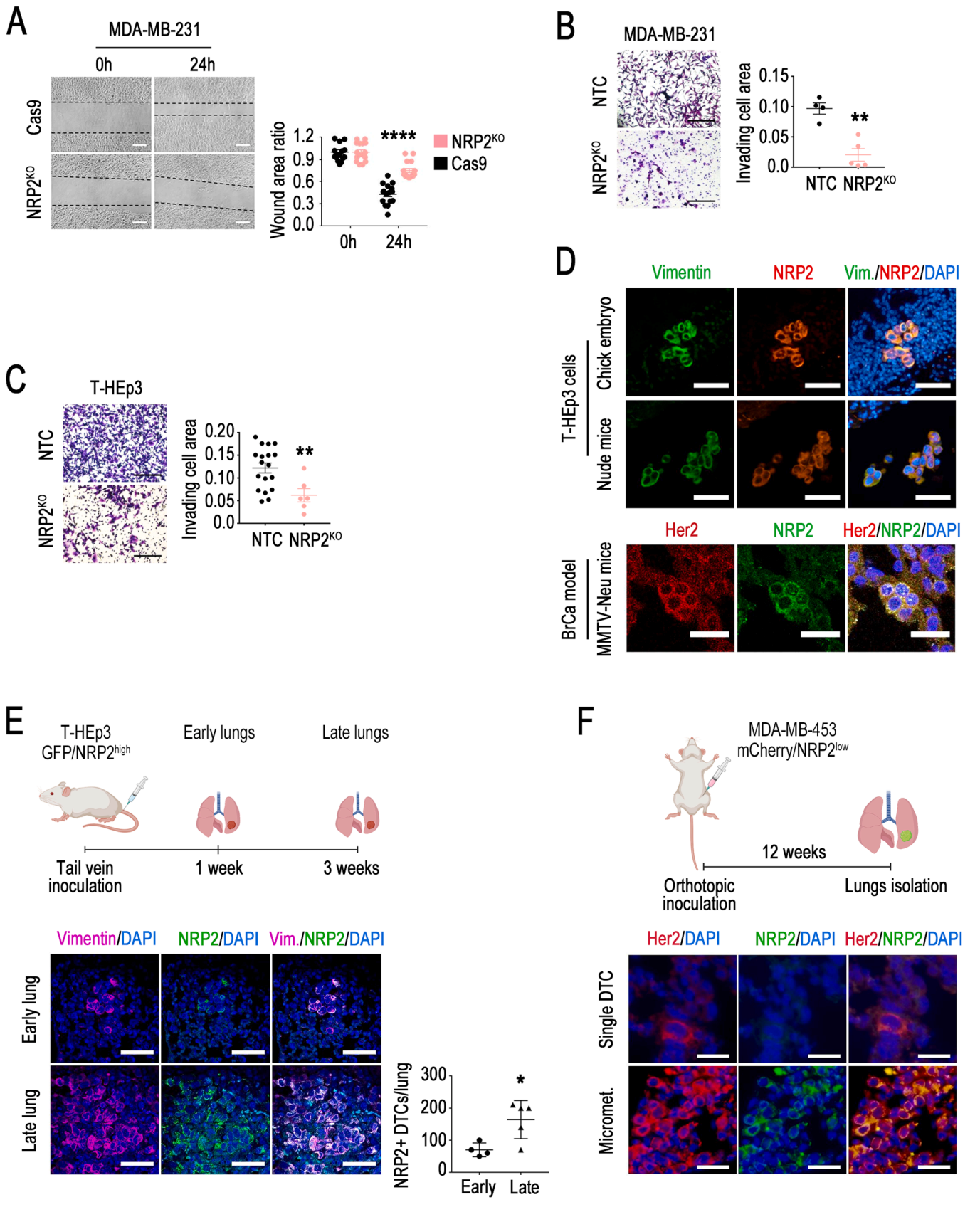
In contrast, treatment of proliferative BrCa and HNSCC cells with TGFβ1, which has been shown to promote DTCs proliferation [7], induced a clear upregulation of NRP2 protein levels (Fig. 4A **and fig. S6C**). Notably, NRP2 levels returned to basal both in BrCa and HNSCC cell lines when treated with the type I TGFβ receptor inhibitor SB431542, implicating the TGFβ1 canonical pathway in NRP2 overexpression (Fig. 4A). Furthermore, TGFβ1 treated 3D-cultured cells showed greater colony formation and higher NRP2 and Ki67 expression (**fig. S6D, E**), further confirming the link between NRP2 expression and proliferation.

These results suggested that the lung microenvironment promotes NRP2 expression. To test this hypothesis, we collected lung-conditioned media (CM) from healthy mouse lungs and used it to stimulate both BrCa and HNSCC proliferative cells. After 24h, we found that NRP2 was highly upregulated in lung CM-treated cells, whereas this effect was partially reversed when the type I TGFβ receptor was inhibited (Fig. 4B).

Next, we checked TGFβ1 levels in lung CM (Fig. 4C). As expected, we found that lung CM was rich in TGFβ1 compared to normal media or MDA-MB-231 and T-HEp3 media (Fig. 4C). To confirm that lung CM upregulation of NRP2 was dependent on TGFβ1, we repeated these experiments using lung CM with partial TGFβ1 depletion (αTGFβ1 lung CM) (Fig. 4D). NRP2 upregulation induced by non-depleted lung CM was partially abrogated in T-HEp3 cells when TGFβ1 was reduced from lung CM (Fig. 4E). Altogether, these results strongly suggest that lung derived TGFβ1 could be a major factor upregulating NRP2 expression in lung DTCs.

Macrophages and fibroblasts have been identified as critical tumor growth-promoting stromal cells in the lung [45,46] and major producers of TGFβ1 within the lung microenvironment [46]. We first verified that THP-1-derived macrophages and CCD19 lung fibroblasts synthetized and released TGFβ1 into the media at higher levels than tumor cells (Fig. 4F). Then, we collected macrophage- and fibroblast-conditioned media and treated the cells with it. In response to stimulation with THP-1 macrophage CM (THP-1 CM), we found that NRP2 expression was markedly increased (Fig. 4G), not only in BrCa and HNSCC proliferative cells, but also in HNSCC lung DTCs (Lu-HEp3) (Fig. 4G). Similarly, CCD19 lung fibroblast CM (CCD19 CM) induced NRP2 overexpression (Fig. 4H). Conversely, inhibition of the canonical TGFβ pathway with the type 1 TGFβ receptor was sufficient to abrogate NRP2 overexpression in all settings (Fig. 4G, H). This indicates that lung fibroblasts and macrophages secrete TGFβ1 which will increase NRP2 expression in tumor cells through a mechanism involving the TGF-β canonical pathway.

It has been described that TGFβ1-driven lung fibrosis promotes dormant lung DTCs re-awakening and generation of overt lung metastases [47]. Therefore, we investigated whether lung fibrosis-induced cancer cell proliferation could be regulated by NRP2. Using young (6 weeks) and old (16 months) mice, we prepared lung CMs and analyzed whether there were differences in NRP2 protein levels in T-HEp3 cells after treatment with these CMs. Higher expression of the activated fibroblast marker α-smooth muscle actin (α-SMA) in old lungs corroborated that they were more fibrotic (Fig. 4I). Consistently, old lungs had higher levels of TGFβ1 (Fig. 4J). When we treated cancer cells with these CMs, both young and old lung CM treatments upregulated NRP2 expression (Fig. 4K). Interestingly, SB431542 treatment reverted NRP2 induction by old lung CM but had little effect on NRP2 induction by young lung CM (Fig. 4K). These results indicate that TGFβ1 regulation of NRP2 induction might be age-dependent, such that TGFβ1, which is more abundant in fibrotic old lungs, could be associated with both NRP2 upregulation and dormant lung DTCs re-awakening. It also raises a question on the relevant contributions of other stromal signals besides TGFβ1, which contribute to the awakening of DTCs in younger lungs.



(caption on next page)

Fig. 3. NRP2 induces cell motility and its expression is up-regulated in lung DTCs and lung metastases *in vivo*. A) Wound healing assay in MDA-MB-231 cells. Left panel, representative images from phase-contrast microscopy. Right panel, quantification of the wound area ratio after 0 and 24h migration in control (Cas9) and $NRP2^{KO}$ MDA-MB-231 cells. Scale bar: 150μm. Graphs represent mean ± S.E.M. (n≥2); ****P < 0.0001, comparing Cas9 *vs* $NRP2^{KO}$ by two-way ANOVA, Sidak's test. **B, C)** Invasion assay in MDA-MB-231 (**B**) and T-HEp3 (**C**) cells. Left panels, representative images from phase-contrast microscopy. Scale bar: 200μm. Right panels, quantification of the invading cells area. Graphs represent mean ± S.E.M. (n=2); **P < 0.01 comparing Cas9/NTC *vs* $NRP2^{KO}$ by *t*-Student's test. **D)** Top and middle panels, representative IF images of vimentin (green) and NRP2 (red) staining of lung T-HEp3 DTCs in chick embryo (top; scale bar: 50μm) and mice (middle; scale bar: 50μm) lung sections. Bottom panel, representative IF images of NRP2 (green) and HER2 (red) staining in MMTV-Neu mice lung sections. Scale bar: 20μm. **E)** Upper panel, diagram of the tail vein *in vivo* injection using T-HEp3 cells. Lower panel, representative IF images of vimentin (pink) and NRP2 (green) in T-HEp3 lung DTCs from early (isolated 1 week post-inoculation) and late (isolated 3 weeks post-inoculation) mice tail vein injection *in vivo* models. Scale bar: 50μm. The graph represents the number of NRP2-positive lung DTCs mean ± S.E.M.; *P < 0.05 comparing early vs late by *t*-Student's test. **F)** Upper panel, diagram of the orthotopic mice *in vivo* experiment using MDA-MB-453 mCherry+ cells. Lower panel, representative IF images of HER2 (red) and NRP2 (green) staining in lung MDA-MB-453 single DTCs and micrometastases (micromets). Scale bar: 50μm.

NRP2 deletion triggers quiescence in lung DTCs in vivo and inhibits lung metastases

Our previous results showed that NRP2 is upregulated in lung DTCs and promotes cell proliferation while inhibiting CDK inhibitors and dormancy regulators (Fig. 1 **and fig. S. 2**). To further uncover the pathological role of NRP2 in lung DTCs biology, we allowed the tumors to grow for 28 days or until they reached $500mm^2$ in the T-HEp3 xenograft model, performed PTs surgery, kept mice for 4 weeks, and isolated lung DTCs (Fig. 5A). Lung DTCs were identified by human vimentin expression (a mesenchymal tumor cell marker), and their phenotype was determined by the proliferation marker Ki67 signal (Ki67-positive, proliferative DTC; Ki67-negative, dormant DTC). We found that lung micrometastases developed from $NRP2^{KO}$ cells were significantly smaller than those in controls (Fig. 5B). Moreover, NRP2 deletion significantly increased the percentage of dormant single-lung DTCs (Fig. 5C).

To rule out that these effects were caused by defects in $NRP2^{KO}$ cells dissemination, invasion, or colonization of secondary organs, as suggested by our observation that $NRP2^{KO}$ cancer cells are less invasive (Fig. 3B-C), we performed a tail vein *in vivo* experiment by inoculating MDA-MB-231, T-HEp3 control (Cas9/NTC), or $NRP2^{KO}$ cells. Lungs were isolated at two and four weeks post-inoculation and cell dissemination was examined (Fig. 5D). In the BrCa model, $NRP2^{KO}$ macrometastases (4 weeks) were significantly smaller than Cas9 macrometastases (Fig. 5E). Moreover, $NRP2^{KO}$ derived DTCs displayed a more dormant phenotype, a prominent effect clearly observed in doublet lung DTCs (Fig. 5F). In the HNSCC model, no macrometastases were found 2 weeks after inoculation (data not shown), while the number of single and double dormant DTCs clearly increased in $NRP2^{KO}$ injected mice at 2 weeks (Fig. 5G). These effects were also evident after four weeks, when a significant reduction in the size of macrometastases was found in $NRP2^{KO}$ mice (Fig. 5H). The number of dormant single and double lung DTCs derived from $NRP2^{KO}$ cells also significantly increased (Fig. 5I). These results suggest that NRP2 plays an important role in lung metastasis development by inhibiting lung DTCs dormancy and promoting the proliferative phenotype of DTCs, thereby favoring the development and enlargement of lung metastases.

NRP2 deletion in head and neck cancer cells upregulates cell cycle regulators expression and inhibits adhesion to the extracellular matrix

To elucidate the biological mechanisms controlled by NRP2 that regulates lung DTCs proliferation, we decided to explore how NRP2 deletion impacts the transcriptional landscape of T-HEp3 HNSCC malignant cells. Principal-component analysis (PCA) of the RNA-seq data across samples showed that replicate samples for each condition are highly similar and that the control and $NRP2^{KO}$ cells are different (**fig. S7A).** Then we conduct a differential expression analysis (DEG) of T-HEp3 *NRP2* depleted cells versus control cells (log2 fold change (FC) < or > 1.5, adjusted p value [p-adj] < 0.05). Out of the total genes analysed, gene expression of 631 genes was significantly altered (Fig. 6A**; Table S2**). A total of 96 genes were found to be upregulated (Fig. 6A-B**; Table S2**). Among the top upregulated genes in $NRP2^{KO}$ cells were Syntaxin Binding Protein 6 (STX6), which enables cadherin binding activity and is involved in cell–cell adhesion. STX6 is predicted to participate in the negative regulation of exocytosis and is localized at adherent junctions [48]. Ankyrin Repeat and Fibronectin Type III Domain Containing 1 (ANKFN1) was also upregulated in $NRP2^{KO}$ cells; this gene has been associated with the regulation of endoplasmic reticulum (ER) stress-related apoptosis pathways. In ovarian cancer, ANKFN1 upregulated apoptotic regulators such as BCL2 and promotes tumour cell survival [49]. Similarly, Endothelial Cell-Specific Molecule 1 (ESM1) was induced in $NRP2^{KO}$ cells. ESM1 is a soluble dermatan sulfate proteoglycan secreted by various cell lines. In hepatocellular carcinoma cells ESM-1 reduced cell survival and proliferation by inducing PTEN-mediated cell cycle arrest [50]. Additionally, upregulation of Musashi RNA Binding Protein 1 (MSI1), a key regulator of post-transcriptional gene expression [51], was observed in $NRP2^{KO}$ cells. Upregulation was also detected for Potassium Channel, Voltage Gated KQT-Like Subfamily Q Member 3 (KCNQ3), which plays a role in the modulation of neuronal excitability [52], and Formin 2 (FMN2), an actin-binding protein implicated in the assembly and reorganization of the actin cytoskeleton [53]. In contrast, 535 genes were downregulated in $NRP2^{KO}$ cells (Fig. 6A-B**; Table S2**). Among the most downregulated genes we found, ATP Binding Cassette Subfamily B Member (TAP1), that has been shown to regulate chemoresistance in colorectal cancer [54]. Retrotransposon Gag Like 1 (RTL1) was also markedly downregulated; Additionally, Prolyl 3-Hydroxylase 2 (P3H2), which plays a crucial role in collagen chain assembly, stability, and cross-linking via post-translational 3-hydroxylation of proline residues [55], was found to be downregulated. Kinesin Family Member 6 (KIF6), a motor protein that is important for the correct segregation of chromosomes and, consequently, maintaining genomic integrity [56], also showed reduced expression in $NRP2^{KO}$ cells. Additionally, Enoyl-CoA Delta Isomerase 2 (ECI2), a key mitochondrial enzyme involved in the β-oxidation of unsaturated fatty acids that has been described to regulate proliferation and survival in prostate cancer [57], was significantly downregulated (Fig. 6A-B**; Table S2**).

Consecutively, a gene ontology (GO) over-representation analysis was performed as shown in Fig. 6C, which revealed that the processes "regulation of cell cycle phase transition" and "mitotic cell cycle phase transition" were over-represented (Fig. 6C), confirming our phenotypic results that deletion of NRP2 reprograms cells into a quiescence / dormant state. Analysis of KEGG pathways also showed over-representation of the signatures "Cell Cycle", "cellular senescence" or "focal adhesion" in $NRP2^{KO}$ cells **(fig. S7B)**.

We explored in more depth the overall expression of genes annotated to the cell cycle regulation ontology and found that most of them were upregulated in $NRP2^{KO}$ cells (**fig. S7C).** Furthermore, gene set enrichment analysis (GSEA) showed that gene signatures of "cell cycle check point signalling" (Normalized Enrichment Score (NES): 2.21618 and FDR q-value: 1.8729708E-4) and "cell cycle signalling" (NES: 1.9176075; FDR q-value: 0.005459815) were strongly and positively associated with deletion of NRP2 (Fig. 6D-E). We have validated the expression of some of the genes included in "Cell Cycle check point

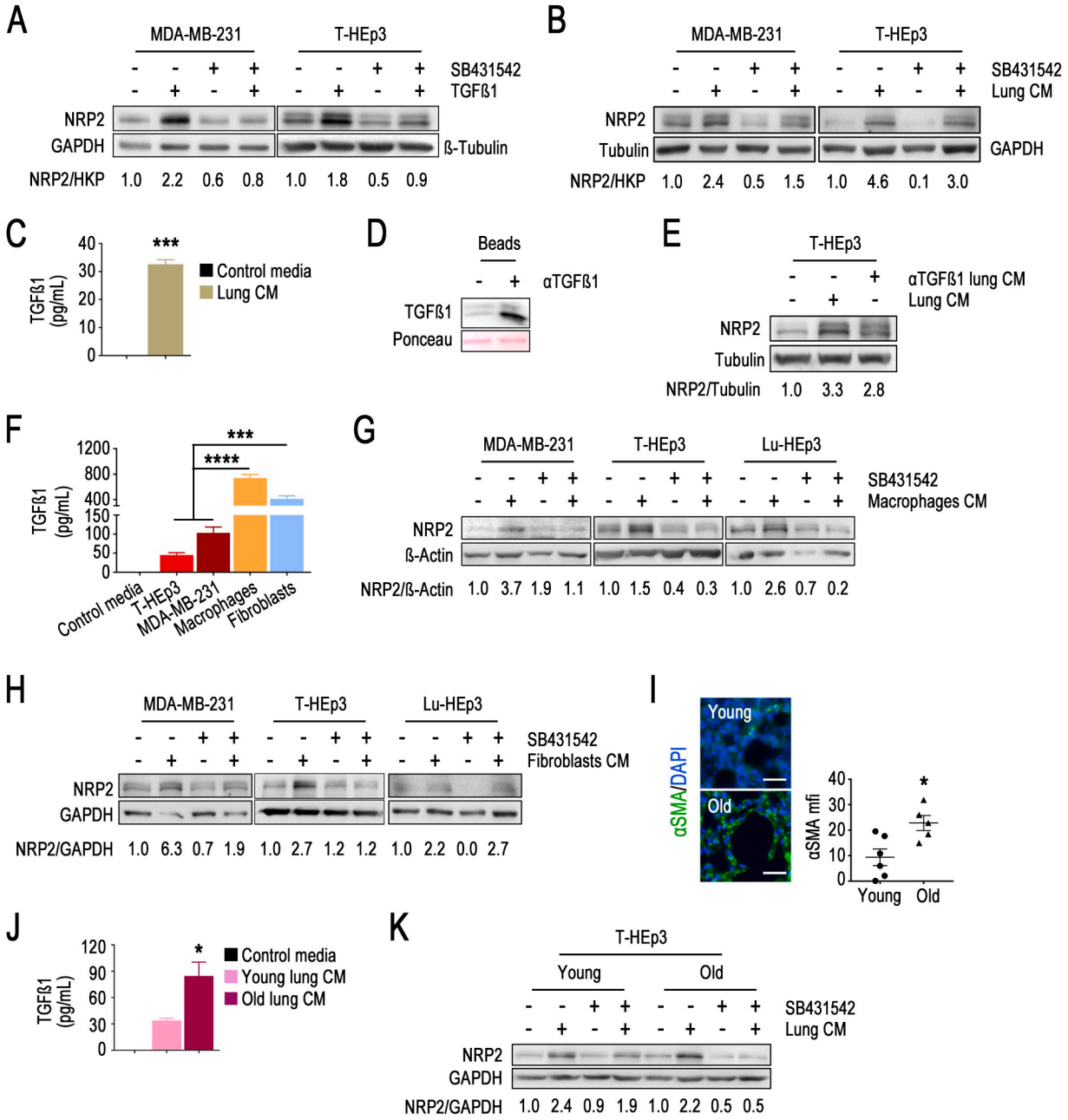


Fig. 4. Lung fibroblasts and macrophages-derived TGFβ1 drives NRP2 up-regulation. A) Representative western blot analysis of NRP2 protein levels normalized with GAPDH or β-tubulin (Housekeeping proteins (HKP)) after 24h treatment with SB431542 (5μM) and/or TGFβ1 (5ng/mL) (n=3). **B)** Representative western blot analysis of NRP2 protein levels normalized with GAPDH or β-tubulin after 24h treatment with lung CM and/or SB431542 (5μM) (n=2). **C)** Quantification of TGFβ1 levels by ELISA (pg/mL) in lung CM. The graph represents the TGFβ1 pg/mL mean values ± S.E.M (n=1, triplicates); ***P < 0.001 comparing control media *vs* lung CM by *t*-Student's test. **D)** Representative western blot analysis of TGFβ1 protein levels released from the beads used for lung CM depletion used in **E**. Beads (-) refers to the control condition where control IgG-bound beads have been used for the assay whereas beads (+) refers to those beads linked to TGFβ1 antibody. **E)** Representative western blot analysis of NRP2 protein levels normalized with tubulin after 24h treatment with lung CM or TGFβ1-depleted lung CM (n=1). **F)** Quantification of TGFβ1 levels by ELISA (pg/mL) in tumor cells (T-HEp3, MDA-MB-231) and TME cells (macrophages, THP-1; fibroblasts, CCD19) conditioned media. The graph represents the TGFβ1 pg/mL mean values ± S.E.M (n=1, triplicates); ***P < 0.001, ****P < 0.0001 comparing tumor cells (T-HEp3 and 231) *vs* THP-1 or CCD19 by one-way ANOVA, Sidak's test. **G, H)** Representative western blot analysis of NRP2 protein levels normalized with GAPDH or β-actin after 24h treatment with macrophages (THP-1) CM and SB431542 (5μM) (**G**) or fibroblasts (CCD19) CM and SB431542 (5μM) (**H**) (n=2). **I)** Left panel, representative IF images of αSMA in young and old mouse lungs (scale bar: 3μm). Right panels, αSMA mfi quantifications. **J)** TGFβ1 quantification by ELISA (pg/mL) in young and old mouse lung CM (n=1, triplicates). Graphs represent mean ± S.E.M.; *P < 0.05 comparing young *vs* old by one-way ANOVA, Sidak's test. **K)** Representative western blot analysis of NRP2 protein levels normalized with GAPDH after 24h treatment with young or old mouse lung CM and SB431542 (5μM) (n=1). In all the western blots, NRP2 protein quantifications are referred to the non-treated control conditions.

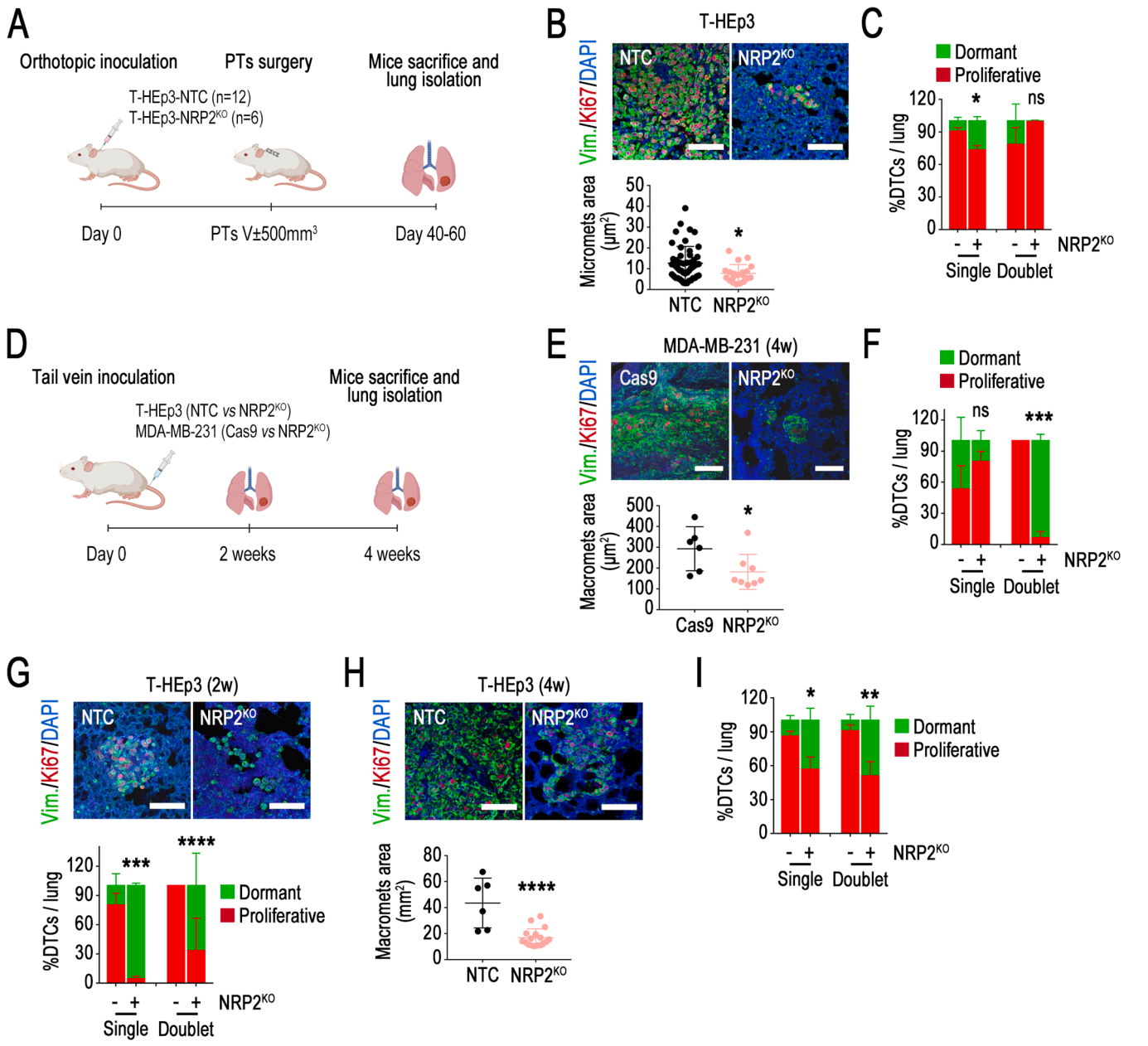
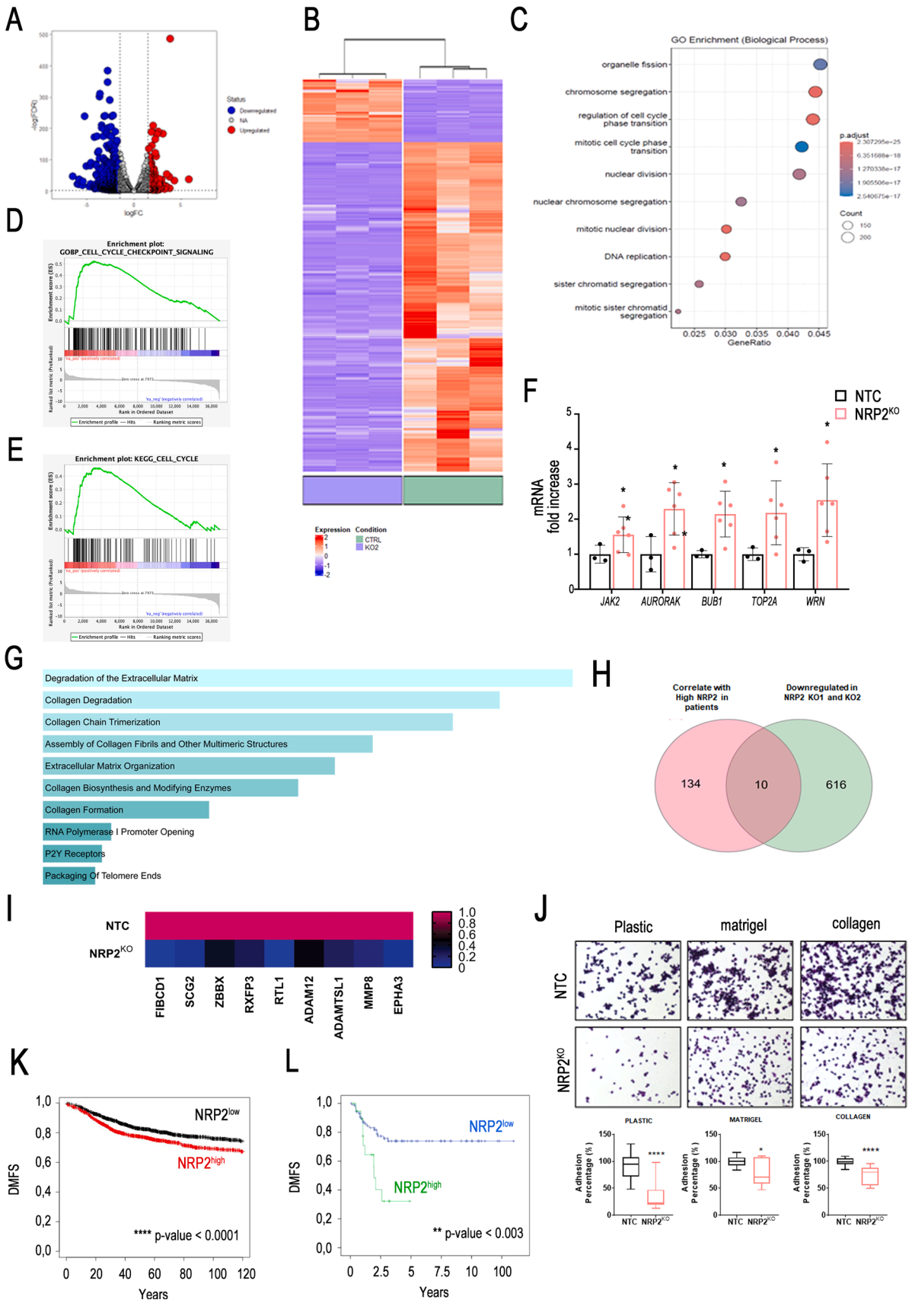


Fig. 5. NRP2 deletion decreases lung metastases size and triggers quiescence in lung DTCs *in vivo*. A) Diagram of the orthotopic mice *in vivo* injection using T-HEp3 cells. **B)** Upper panel, representative IF images of vimentin (Vim.; green) and Ki67 (red) staining of T-HEp3 lung DTCs (scale bar: 100µm). Lower panel, quantification of lung micrometastases area (µm^2) using ImageJ software. **C)** Quantification of the percentage (%) of Ki67-positive (proliferative) or Ki67-negative (dormant) single and doublet T-HEp3 cells per lung. **D)** Diagram of the tail vein mice *in vivo* injection using MDA-MB-231 or T-HEp3 cells. **E)** Upper panel, representative IF images of vimentin (Vim.; green) and Ki67 (red) staining of MDA-MB-231 lung DTCs 4 weeks (4w) after inoculation (scale bar: 50µm). Lower panel, quantification of lung macrometastases area (µm^2) using ImageJ software. **F)** Quantification of the % of Ki67-positive or Ki67-negative single and doublet MDA-MB-231 cells per lung. **G)** Upper panel, representative IF images of vimentin (Vim.; green) and Ki67 (red) staining of T-HEp3 lung DTCs 2 weeks (2w) after inoculation (scale bar: 50µm). Lower panel, quantification of the % of Ki67-positive or Ki67-negative single and doublet T-HEp3 cells per lung. **H)** Upper panel, representative IF images of vimentin (Vim.; green) and Ki67 (red) staining of T-HEp3 lung DTCs 4 weeks (4w) after inoculation (scale bar: 50µm). Lower panel, quantification of lung macrometastases area (mm^2) using ImageJ software. **I)** Quantification of the % of Ki67-positive or Ki67-negative single and doublet T-HEp3 cells per lung. Graphs represent mean ± S.E.M. (n≥5 lungs per group); ns, non-significant, *P < 0.05, **P < 0.01, ***P < 0.001, ****P < 0.0001 comparing NTC *vs* NRP2^{KO} by *t*-Student's test.

signalling" term by RTqPCR (Fig. 6F). Our results showed that Janus kinase 2 (*JAK2*), Aurora kinase (*AURORAK*), DNA Topoisomerase II Alpha (*TOP2A*), BUB1 Mitotic Checkpoint Serine/Threonine Kinase (*BUB1*) and Werner Syndrome ATP-Dependent Helicase (*WRN*) are all upregulated in NRP2^{KO} cells. This suggests that NRP2 deletion impairs proliferation of metastatic cells by inducing the expression of cell cycle regulatory pathways and promoting DTCs quiescence. Interestingly, the GSEA analysis also showed that the processes related to growth factor binding (NES:-1.7011257; FDR q-value: 0.04983139) and G protein coupled receptors (GPCR) ligand binding (NES:-1.652787; FDR q-value: 0.11120763) were inversely correlated with deletion of NRP2 (**fig. S7D-E**). Hence, our results strongly suggest that deletion of NRP2 reprograms cells into a dormant state that reduces proliferation signaling through upregulation of several cell cycle inhibitors and cell cycle check point regulators and downregulates growth factor signaling.

Additionally, we performed a GO analysis of the downregulated



(caption on next page)

Fig. 6. NRP2 deletion induces the expression of genes involved in cell cycle regulation and inhibits the expression of genes involved in remodeling of the extracellular matrix. A) Volcano plot showing the genes induced (red) and repressed (blue) in NRP2 KO cells. **B)**-Heat map that shows the genes differentially expressed between NRP2 KO and NTC cells. **C)** GO biological pathway enrichment analysis (GO:BP) using biological process databases for the genes differentially expressed between NTC and NRP2^{KO} cells. **D-E)** GSEA analysis in the GO biological process (**D**) and Kegg pathways (**E**) databases. Enrichment score (ES) plots for the indicated gene sets in the top most up-regulated genes in NRP2^{KO} cells. Vertical bars refer to individual genes in a gene set and their position reflects the contribution of each gene to the ES. **F)** Analysis of *JAK2, AURORAK, TOP2A, BUB1 and WRN* mRNA relative expression in T-HEp3 NTC and *NRP2*-deleted (NRP2^{KO}) cells after 24h. The bar plot shows relative quantification (RQ) values referred to the NTC cells (n=3). The graph represents RQ mean values ± S.E.M.; *P < 0.05 by *Mann Whitney* test. **G)** Analysis of overrepresentation of downregulated genes in NRP2^{KO} cells (p-adjusted value < 0.05, FC<0.5) in the databases "*Reactome*". The top 10 terms with the highest gene proportion are represented with a p-adjusted cut-off value of 0.05 and redundant terms removed. **H)** Venn diagram showing the genes whose expression correlates with high NRP2 expression in RNA sequencing data from head and neck cancer patient samples and downregulated genes in NRP2^{KO} cells. **I)** Heat map showing the expression of genes in common between those correlated with high NRP2 expression in patients and those inhibited in NRP2-deficient cells. **J)** Representative images of adhesion of T-HEp3 NTC and NRP2^{KO} cells to plastic, matrigel and collagen after 30 min. The graphs represent the mean value of the percentage of adhesion to plastic, matrigel and collagen ± S.D with respect to NTC cells (n=3, per sixfold for plastic /n=4, per sixfold for matrigel and collagen). **K)** Kaplan-Meier curve for distant metastases-free survival (DMFS) in a cohort of 2765 BrCa patients with high (red; n=1437) or low (black; n=1328) levels of NRP2. . **L)** Kaplan-Meier curve for DMFS in a cohort of 92 HNSCC patients with high (green; n=20) or low (blue; n=72) levels of NRP2. Analysis performed in collaboration with Dr. Camacho and Dr. Leon from Santa Creu i Sant Pau Hospital (Barcelona, Spain).

genes in NRP2^{KO} cells (**Table S2**) and found that they participate in extracellular matrix regulation and collagen synthesis regulation pathways (Fig. 6G, **Table S2**). This correlates with the data we had previously obtained when analysing RNA sequencing data from patients (downloaded from the TCGA), where we had observed that NRP2 expression positively correlated with extracellular matrix remodelling both in head and neck and breast cancer patient samples (**fig. S7H-I**). By cross-referencing the genes whose expression correlates with that of NRP2 in patients and the genes downregulated in NRP2^{KO} cells, we obtained a list of 9 common genes (Fig. 6H-I). These genes are primarily involved in the regulation of the extracellular matrix (**fig. S7J**). These results suggest that NRP2 promotes DTCs proliferation by fostering extracellular cell matrix adhesion and binding of growth factors to their receptors. To confirm this, we have analysed the role of NRP2 in the interaction with the extracellular matrix. Our results show that the absence of NRP2 inhibits adhesion to different components of the extracellular matrix including collagen (Fig. 6J) in agreement with the results of our transcriptomic analysis.

High levels of NRP2 negatively correlate with BrCa and HNSCC patients' distant metastases free survival

The initial characterization of NRPs expression revealed the upregulation of NRP2 in the more aggressive BrCa and HNSCC cell lines (Fig. 1A-D). In addition, previous data from our group have shown that NRP2 expression correlates with worse prognosis in patients with BrCa [17]. Analysis of a cohort of 2765 BrCa patients using the Kaplan-Meier plot database [26] showed that patients with high NRP2 expression had shorter distant metastasis-free survival (DMFS) periods (61.2 months) than those with low NRP2 expression (116 months) (Fig. 6K). Similarly, higher levels of NRP2 were positively correlated with a higher risk of developing metastasis and with worse DMFS in a cohort of 92 HNSCC patients (Fig. 6L). Therefore, these results revealed that NRP2 expression correlates with a higher risk of metastasis development, identifying it as a suitable biomarker candidate for metastatic risk.

DISCUSSION

Signaling crosstalk between sympathetic, parasympathetic, or sensory nerves and nervous system-related factors in the TME and tumor cells regulates cancer initiation, progression, or metastasis of various cancers, including pancreatic, gastric, colon, prostate breast, oral, and skin cancers, often through neurotransmitters, neuropeptides, and axon guidance-dependent signaling cascades [11,13,22,58,59]. Specifically, our data showed that NRP2 expression protects tumor cells from apoptosis and predisposes them to escape from dormancy and proliferate both in the primary tumor and in the context of lung metastasis. Moreover, our results strongly support that NRP2-dependent proliferation enhancement is mediated through inhibition of dormancy and cell cycle regulators such as p27Kip1. In addition, we found that NRP2-dependent tumor-promoting effects in lung metastases require stromal TGFβ1, which is largely secreted by lung fibroblasts and macrophages and remodeling of the extracellular matrix.

Our results revealed a tumor-promoting function of NRP2 in both basal BrCa and HNSCC (Fig. 1, 2) by inhibiting tumor cell quiescence, promoting colony formation, and proliferation both *in vitro* and *in vivo*. In agreement with our results, NRP2 has been shown to play a key role in tumor growth by regulating several tumorigenic processes, such as cell proliferation [19]. In general, high levels of NRP2 have been associated with more proliferative breast [17], lung [60], melanoma [61], colorectal [62] and head and neck [63] tumors. However, the mechanism by which NRP2 induces cell proliferation is not well understood.

Here, we show that NRP2 fosters proliferation through downregulation of dormancy regulators such as *TGFBR3* [7] or *NR2F1/Sox9/RARβ* [37] and cell cycle check point inhibitors such as p21 and p27. In concordance with our data, NRP1 depletion downregulated Ki67 levels and induced p27 expression and cell cycle arrest in gastric cancer [64], although the mechanisms underlying the regulation of p27 by NRPs remain unknown. There may be other mechanisms underlying the association between NRP2 and cell proliferation. Our results also showed that deletion of NRP2, downregulates pathways related to extracellular matrix remodeling and collagen organization (fig.6 **and fig. S7**) suggesting that NRP2 might be regulating DTCs adaptation to secondary organs, facilitating their interaction with the extracellular matrix NRP2 has previously been reported to interact with integrins and other components of the extracellular matrix [40,65]. In our transcriptomic analysis we found mostly changes in proteins related to collagen organization such as P3H2. Interestingly collagen organization has been previously related with activation of dormant DTCs in the lung [66]. Hence, we propose that NRP2 might facilitate the interaction of DTCs with the lung microenvironment, promoting adhesion and collagen reorganization, and fostering DTCs awakening from dormancy. Interestingly, analysis of patient databases showed that NRP2 expression correlates with genes involved in extracellular matrix remodeling both in head and neck and breast cancer patients (**fig. S7**) which supports our conclusions.

Our results show that NRP2 also promotes cancer cell invasion and dissemination (Fig. 3, 5), which is in agreement with previous reports that NRP2 regulates endothelial and tumor cell migration [40,62,63]. Interestingly, our study revealed for the first time that lung DTCs overexpress NRP2, and that its expression is required to drive cancer cell proliferation to form metastases (Fig. 3). These data suggest that the lung microenvironment selectively regulates NRP2 expression in DTCs. Studies on lung cancer have consistently demonstrated that the lung microenvironment positively regulates NRP2, but not NRP1 expression [60]. Among the known NRP2 regulators, we found that NRP2 overexpression was selectively elicited by TGFβ1, but not by VEGF-C or SEMF3F. Moreover, this overexpression was partially abrogated by an

inhibitor of the canonical TGFβ1 pathway, implicating TGF-β receptor activation of SMAD2/SMAD3 in this process. Consistently, Nasarre *et al* showed that NRP2 was upregulated by TGFβ1 [60] and a recent study showed that SMAD3 increases NRP2 expression by binding to its mRNA 5' untranslated region [67]. In addition, genetic or chemical inhibition of SMAD4 also decreases NRP2 levels, impairing tumor cell migration [62]. Conversely, NRP2 upregulation has also been described as a SMAD-independent process involving the ERK and AKT signaling pathways [60,63]. In our model, we found that NRP2 upregulation was partly reversed by TGFβ receptor I inhibition or TGFβ I depletion, suggesting that NRP2 regulation in lung DTCs is partly dependent on the TGFβ1 canonical pathway.

Our results indicate that lung fibroblasts and macrophages-derived TGFβ1 induces NRP2 expression. Inhibition or ablation of lung macrophages reduces the burden of BrCa metastases [68], even when metastases are already established [69], confirming the requirement of macrophages for lung metastatic seeding and growth. This agrees with our results that show that macrophage production of TGFβ1 upregulates NRP2 expression in lung DTCs, promoting DTCs reprogramming from dormancy to proliferation and progression to metastasis growth. It has also been shown that the composition of the stroma determines the fate of DTCs, where type I and III collagen and fibronectin induce the proliferation of dormant BrCa DTCs that develop proliferative lung metastatic lesions [47,66,70]. The most abundant factor secreted by activated fibroblasts is TGFβ1 [71]. Accordingly, we found that CCD19-LU lung fibroblasts synthetized and secreted TGFβ1 into the media. TGFβ1 has already been shown to promote the re-awakening of dormant BrCa DTCs [7,8,47]. Here, we have additionally shown that old and fibrotic lung-derived TGFβ1 up-regulates NRP2 expression, suggesting that NRP2 might play a crucial role in cell quiescence inhibition and proliferation activation in fibrotic lungs. In agreement with this, Fane et al. recently showed that an aged lung microenvironment facilitates the outgrowth of dormant melanoma DTCs [72]. Although the detailed mechanisms are undefined, previous work suggests that the Wnt pathway may be implicated, since in TGFβ1-mediated fibrosis, the canonical Wnt pathway is activated, which in turn stimulates fibroblast differentiation and activation [73] and blocking canonical Wnt signaling downregulates NRP2 expression [74], resulting in the suppression of tumor growth and lung metastasis [75].

Finally, our results revealed that NRP2 expression correlates with worse prognosis and a higher risk of developing metastases in both breast and head and neck cancers. This is in agreement with a recent report from Kang *et al.*, who also showed that high expression of NRP2 correlated with lymph node metastasis and distant metastasis in patients with esophageal squamous cell carcinoma (OSCC) [76] and with our previous data, where we showed that high expression of SEMA3F and NRP2 correlated with occult lymph node metastasis in HNSSC [18] and that high expression of NRP2 is associated with worse prognosis in BrCa [17]. In fact, knocking out NRP2 expression decreased the size of micrometastases and, more interestingly, reprogramed single DTCs to quiescence in both HNSCC and BrCa models (Fig. 5). Some reports have suggested a role for NRP2 in cancer metastasis [77]. For instance, NRP2 promotes metastasis in OSCC through deregulation of the ERK-MAPK-ETV4-MMP-E-cadherin pathway [63]. In another study, NRP2 interaction with integrin-β1 promoted FAK/ERK/HIF-1α/VEGF signaling favoring metastasis [65]. In BrCa, inhibition of NRP2 using a blocking antibody has been shown to prevent tumor lymphangiogenesis and metastasis, in part by modulating VEGFR3 signaling [77]. In our study, NRP2 promotes lung metastasis formation through inhibition of several dormancy regulators and cell cycle checkpoint inhibitors, which trigger DTCs escape from dormancy and their switch into proliferative behavior. Furthermore, NRP2 also promotes extracellular cell matrix remodeling and facilitates lung DTCs adhesion to collagen favoring metastasis. Overall, our results show that stromal TGFβ1 induces NRP2 expression, which protects lung DTCs from apoptosis, promotes the interaction of lung DTCs with the extracellular matrix and induces the reprogramming of lung DTCs into a proliferative phenotype, thereby increasing lung metastasis development. Our findings have potential clinical implications and may lead to the use of NRP2 as a biomarker to predict tumor recurrence as well as a therapeutic intervention target to reduce metastasis dissemination and outgrowth through NRP2 inhibition.

Data and materials availability

All data are available in the main text or the supplemental materials.

Funding

All funding was cosponsored by the European FEDER Program. L.R-P., I. dlG.-L., N.P. and S.M. were recipients of FPU fellowships from the Spanish Ministry of Education. A.G-U. and M.R. are supported by the Madrid Community Program for Talent Attraction (2017-T1/BMD-5468). P.F.-N. is supported by a Juan de la Cierva contract from the Spanish Ministry of science, innovation, and universities. P.F.-N. and G. F. are supported by the Cellex Foundation. P.F.-N., G.F., N.C., and P.G. are funded by La Marató TV3 (201915-30-31), and by Secretaria d'Universitats i Recerca del Departament d'Economia i Coneixement (2017_SGR_1305). P.B. received support from BBVA (Becas Leonardo 2018, BBM-TRA-0041). J.A.A-G was supported by The National Institute of Health /National Cancer Institute (Grant CA109182) and the Samuel Waxman Cancer Research Foundation Tumor Dormancy Program. E.D. was funded by The National Institute of Health /National Cancer Institute (T32 CA078207). M. I.-G and P. L-A. are supported by a predoctoral contract from Comunidad de Madrid. M. C.-R. is a recipient of a predoctoral contract from UCM.

CRediT authorship contribution statement

L Recalde-Percaz: Writing – original draft, Methodology, Investigation, Formal analysis, Conceptualization. **I de la Guia-Lopez:** Investigation. **P Linzoain-Agos:** Investigation. **A Noguera-Castells:** Investigation. **M Rodrigo-Faus:** Investigation. **P Jauregui:** Methodology, Investigation. **A Lopez-Plana:** Investigation. **P Fernández-Nogueira:** Investigation. **M Iniesta-González:** Investigation. **M Cueto-Remacha:** Investigation. **S Manzano:** Investigation. **R Alonso:** Methodology, Investigation. **N Moragas:** Investigation. **C Baquero:** Investigation. **N Palao:** Investigation. **E Dalla:** Investigation. **FX Avilés-Jurado:** Resources. **I Vilaseca:** Resources. **X León-Vintró:** Resources, Formal analysis. **M Camacho:** Resources, Formal analysis. **G Fuster:** Writing – review & editing, Investigation. **J Alcaraz:** Writing – review & editing, Resources. **J Aguirre-Ghiso:** Writing – review & editing, Resources. **P Gascón:** Writing – review & editing, Resources, Funding acquisition, Conceptualization. **A Porras:** Writing – review & editing. **A Gutiérrez-Uzquiza:** Writing – review & editing, Resources. **N Carbó:** Supervision, Resources. **P Bragado:** Writing – review & editing, Writing – original draft, Visualization, Supervision, Funding acquisition, Formal analysis, Conceptualization.

Declaration of competing interest

The authors declare the following financial interests/personal relationships which may be considered as potential competing interests: JAAG is a scientific co-founder and scientific advisory board member and equity owner in HiberCell and receives financial compensation as a consultant for HiberCell, a Mount Sinai spin-off company focused on the research and development of therapeutics that prevent or delay the recurrence of cancer.

All other authors declare they have no competing interests.

Acknowledgements

The authors thank Darya Kulyk for her help preparing the schemes that are shown in the figures. This work was supported by grants from the Spanish Ministry of Economy and Competitiveness [PID2019-104991RB-I00 and PID2022-136959OB-I00 to P.B., PID2019-104143RB-C22 and PID2022-137717OB-C21 to A.P and CNS 2023-144109 and PID2020117650RAI00 to A.G.-U,.].

Supplementary materials

Supplementary material associated with this article can be found, in the online version, at doi:10.1016/j.neo.2025.101220.

References

[1] D.R. Welch, D.R. Hurst, Defining the hallmarks of metastasis, Cancer. Res 79 (2019) 3011–3027.
[2] M.S. Sosa, P. Bragado, J.A. Aguirre-Ghiso, Mechanisms of disseminated cancer cell dormancy: an awakening field, Nat. Rev. Cancer 14 (2014) 611.
[3] J.A. Aguirre-Ghiso, Models, mechanisms and clinical evidence for cancer dormancy, Nat. Rev. Cancer 7 (2007) 834–846.
[4] R.R. Gomis, S. Gawrzak, Tumor cell dormancy, Mol. Oncol 11 (2017) 62–78.
[5] L. Mathot, J. Stenninger, Behavior of seeds and soil in the mechanism of metastasis: a deeper understanding, Cancer. Sci 103 (2012) 626–631.
[6] S. Paget, The distribution of secondary growths in cancer of the breast, 1889, Cancer. Metastasis. Rev 8 (1989) 98–101.
[7] P. Bragado, Y. Estrada, F. Parikh, S. Krause, C. Capobianco, H.G. Farina, D. M. Schewe, J.A. Aguirre-Ghiso, TGF-beta2 dictates disseminated tumour cell fate in target organs through TGF-beta-RIII and p38alpha/beta signalling, Nat. Cell. Biol 15 (2013) 1351–1361.
[8] C.M. Ghajar, H. Peinado, H. Mori, I.R. Matei, K.J. Evason, H. Brazier, D. Almeida, A. Koller, K.A. Hajjar, D.Y. Stainier, et al., The perivascular niche regulates breast tumour dormancy, Nat. Cell. Biol 15 (2013) 807–817.
[9] K. Yumoto, M.R. Eber, J. Wang, F.C. Cackowski, A.M. Decker, E. Lee, A.R. Nobre, J. A. Aguirre-Ghiso, Y. Jung, R.S. Taichman, Axl is required for TGF-beta2-induced dormancy of prostate cancer cells in the bone marrow, Sci. Rep 6 (2016) 36520.
[10] A. Kobayashi, H. Okuda, F. Xing, P.R. Pandey, M. Watabe, S. Hirota, S.K. Pai, W. Liu, K. Fukuda, C. Chambers, et al., Bone morphogenetic protein 7 in dormancy and metastasis of prostate cancer stem-like cells in bone, J. Exp. Med 208 (2011) 2641–2655.
[11] M. Mancino, E. Ametller, P. Gascon, V. Almendro, The neuronal influence on tumor progression, Biochim. Biophys. Acta 1816 (2011) 105–118.
[12] S.W. Cole, A.S. Nagaraja, S.K. Lutgendorf, P.A. Green, A.K. Sood, Sympathetic nervous system regulation of the tumour microenvironment, Nat. Rev. Cancer 15 (2015) 563–572.
[13] C. Magnon, S.J. Hall, J. Lin, X. Xue, L. Gerber, S.J. Freedland, P.S. Frenette, Autonomic nerve development contributes to prostate cancer progression, Science 341 (2013) 1236361.
[14] C.M. Zhao, Y. Hayakawa, Y. Kodama, S. Muthupalani, C.B. Westphalen, G. T. Andersen, A. Flatberg, H. Johannessen, R.A. Friedman, B.W. Renz, et al., Denervation suppresses gastric tumorigenesis, Sci. Transl. Med 6 (2014) 250ra115.
[15] G. Pascual, D. Domínguez, M. Elosúa-Bayes, F. Beckedorff, C. Laudanna, C. Bigas, D. Douillet, C. Greco, A. Symeonidi, I. Hernández, et al., Dietary palmitic acid promotes a prometastatic memory via Schwann cells, Nature 599 (2021) 485–490.
[16] A.M. Decker, Y. Jung, F.C. Cackowski, K. Yumoto, J. Wang, R.S. Taichman, Sympathetic signaling reactivates quiescent disseminated prostate cancer cells in the bone marrow, Mol. Cancer. Res 15 (2017) 1644–1655.
[17] P. Fernandez-Nogueira, P. Bragado, V. Almendro, E. Ametller, J. Rios, S. Choudhury, M. Mancino, P. Gascon, Differential expression of neurogenes among breast cancer subtypes identifies high risk patients, Oncotarget 7 (2016) 5313–5326.
[18] C. Meler-Claramonte, F.X. Aviles-Jurado, I. Vilaseca, X. Terra, P. Bragado, G. Fuster, Vintro X Leon, M. Camacho, Semaphorin-3F/neuropilin-2 transcriptional expression as a predictive biomarker of occult lymph node metastases in HNSCC, Cancers. (Basel) (2022) 14.
[19] G.J. Prud'homme, Y. Glinka, Neuropilins are multifunctional coreceptors involved in tumor initiation, growth, metastasis and immunity, Oncotarget 3 (2012) 921–939.
[20] C. Raimondi, C. Ruhrberg, Neuropilin signalling in vessels, neurons and tumours, Semin. Cell. Dev. Biol 24 (2013) 172–178.
[21] P. Fernandez-Nogueira, M. Mancino, G. Fuster, A. Lopez-Plana, P. Jauregui, V. Almendro, E. Enreig, S. Menendez, F. Rojo, A. Noguera-Castells, et al., Tumor-associated fibroblasts promote HER2-targeted therapy resistance through FGFR2 activation, Clin. Cancer. Res 26 (2020) 1432–1448.
[22] A. Zubeldia-Plazaola, L. Recalde-Percaz, N. Moragas, M. Alcaraz, X. Chen, M. Mancino, P. Fernandez-Nogueira, de Puig M Prats, F. Guzman, A. Noguera-Castells, et al., Glucocorticoids promote transition of ductal carcinoma in situ to invasive ductal carcinoma by inducing myoepithelial cell apoptosis, Breast. Cancer. Res 20 (2018) 65.
[23] O. Shalem, N.E. Sanjana, E. Hartenian, X. Shi, D.A. Scott, T. Mikkelson, D. Heckl, B. L. Ebert, D.E. Root, J.G. Doench, et al., Genome-scale CRISPR-Cas9 knockout screening in human cells, Science 343 (2014) 84–87.
[24] K.L. Harper, M.S. Sosa, D. Entenberg, H. Hosseini, J.F. Cheung, R. Nobre, A. Avivar-Valderas, C. Nagi, N. Girnius, R.J. Davis, et al., Mechanism of early dissemination and metastasis in Her2(+) mammary cancer, Nature 540 (2016) 588–592.
[25] M. Ringner, E. Fredlund, J. Hakkinen, A. Borg, J. Staaf, GOBO: gene expression-based outcome for breast cancer online, PLoS. One 6 (2011) e17911.
[26] A. Nagy, G. Munkacsy, B. Gyorffy, Pancancer survival analysis of cancer hallmark genes, Sci. Rep 11 (2021) 6047.
[27] Team RC (2025). *R: A language and environment for statistical computing. R Foundation for Statistical Computing,* Vienna, Austria. *URL:* https://www.R-project.org. Editor (ed)^(eds): City.
[28] M.I. Love, W. Huber, S. Anders, Moderated estimation of fold change and dispersion for RNA-seq data with DESeq2, Genome. Biol 15 (2014) 550.
[29] T. Wu, E. Hu, S. Xu, M. Chen, P. Guo, Z. Dai, T. Feng, L. Zhou, W. Tang, L. Zhan, et al., clusterProfiler 4.0: A universal enrichment tool for interpreting omics data, Innov. (Camb) 2 (2021) 100141.
[30] M. Carlson, S. Falcon, H. Pages, N. Li, org. Hs. eg. db: genome wide annotation for Human, R. package. version 3 (2019) 3.
[31] S. Sayols, rrvgo: a bioconductor package for interpreting lists of gene ontology terms, MicroPubl. Biol (2023). **2023**.
[32] H W (2016). *ggplot2: Elegant graphics for Data analysis.*, Vol. Springer-Verlag New York.
[33] A. Subramanian, P. Tamayo, V.K. Mootha, S. Mukherjee, B.L. Ebert, M.A. Gillette, A. Paulovich, S.L. Pomeroy, T.R. Golub, E.S. Lander, et al., Gene set enrichment analysis: a knowledge-based approach for interpreting genome-wide expression profiles, Proc. Natl. Acad. Sci. U. S. A 102 (2005) 15545–15550.
[34] R.S. Kim, A. Avivar-Valderas, Y. Estrada, P. Bragado, M.S. Sosa, J.A. Aguirre-Ghiso, J.E. Segall, Dormancy signatures and metastasis in estrogen receptor positive and negative breast cancer, PLoS. One 7 (2012) e35569.
[35] A.P. Adam, A. George, D. Schewe, P. Bragado, B.V. Iglesias, A.C. Ranganathan, A. Kourtidis, D.S. Conklin, J.A. Aguirre-Ghiso, Computational identification of a p38SAPK-regulated transcription factor network required for tumor cell quiescence, Cancer. Res 69 (2009) 5664–5672.
[36] O. Coqueret, New roles for p21 and p27 cell-cycle inhibitors: a function for each cell compartment? Trends. Cell. Biol 13 (2003) 65–70.
[37] M.S. Sosa, F. Parikh, A.G. Maia, Y. Estrada, A. Bosch, P. Bragado, E. Ekpin, A. George, Y. Zheng, H-M Lam, et al., NR2F1 controls tumour cell dormancy via SOX9- and rarβ-driven quiescence programmes, Nat. Commun. 6 (2015) 6170.
[38] J.A. Aguirre-Ghiso, Y. Estrada, D. Liu, L. Ossowski, ERK(MAPK) activity as a determinant of tumor growth and dormancy; regulation by p38(SAPK), Cancer. Res 63 (2003) 1684–1695.
[39] A. Fantozzi, G. Christofori, Mouse models of breast cancer metastasis, Breast. Cancer. Res 8 (2006) 212.
[40] A.A.A. Alghamdi, C.J. Benwell, S.J. Atkinson, J. Lambert, R.T. Johnson, S. D. Robinson, NRP2 as an emerging angiogenic player; promoting endothelial cell adhesion and migration by regulating recycling of alpha5 integrin, Front. Cell. Dev. Biol 8 (2020) 395.
[41] P. Wittmann, M. Grubinger, C. Groger, H. Huber, W. Sieghart, M. Peck-Radosavljevic, W. Mikulits, Neuropilin-2 induced by transforming growth factor-beta augments migration of hepatocellular carcinoma cells, BMC. Cancer 15 (2015) 909.
[42] J. Wang, Y. Huang, J. Zhang, B. Xing, W. Xuan, H. Wang, H. Huang, J. Yang, J. Tang, NRP-2 in tumor lymphangiogenesis and lymphatic metastasis, Cancer. Lett 418 (2018) 176–184.
[43] R.J. Giger, J.F. Cloutier, A. Sahay, R.K. Prinjha, D.V. Levengood, S.E. Moore, S. Pickering, D. Simmons, S. Rastan, F.S. Walsh, et al., Neuropilin-2 is required in vivo for selective axon guidance responses to secreted semaphorins, Neuron 25 (2000) 29–41.
[44] P. Nasarre, R.M. Gemmill, H.A. Drabkin, The emerging role of class-3 semaphorins and their neuropilin receptors in oncology, Onco. Targets. Ther 7 (2014) 1663–1687.
[45] M. Casanova-Acebes, E. Dalla, A.M. Leader, J. LeBerichel, J. Nikolic, B.M. Morales, M. Brown, C. Chang, L. Troncoso, S.T. Chen, et al., Tissue-resident macrophages provide a pro-tumorigenic niche to early NSCLC cells, Nature 595 (2021) 578–584.
[46] R. Ikemori, M. Gabasa, P. Duch, M. Vizoso, P. Bragado, M. Arshakyan, I.C. Luis, A. Marin, S. Moran, M. Castro, et al., Epigenetic SMAD3 repression in tumor-associated fibroblasts impairs fibrosis and response to the antifibrotic drug Nintedanib in lung squamous cell carcinoma, Cancer. Res 80 (2020) 276–290.
[47] D. Barkan, L.H. El Touny, A.M. Michalowski, J.A. Smith, I. Chu, A.S. Davis, J. D. Webster, S. Hoover, R.M. Simpson, J. Gauldie, et al., Metastatic growth from dormant cells induced by a col-I-enriched fibrotic environment, Cancer. Res 70 (2010) 5706–5716.
[48] Y. Zhang, L. Shu, X. Chen, Syntaxin 6, a regulator of the protein trafficking machinery and a target of the p53 family, is required for cell adhesion and survival, J. Biol. Chem 283 (2008) 30689–30698.
[49] Y. Lei, B.R. Henderson, C. Emmanuel, P.R. Harnett, A. deFazio, Inhibition of ANKRD1 sensitizes human ovarian cancer cells to endoplasmic reticulum stress-induced apoptosis, Oncogene 34 (2015) 485–495.
[50] Y.H. Kang, N.Y. Ji, C.I. Lee, H.G. Lee, J.W. Kim, Y.I.L. Yeom, D.G. Kim, S.K. Yoon, J.W. Kim, P.J. Park, et al., ESM-1 silencing decreased cell survival, migration, and invasion and modulated cell cycle progression in hepatocellular carcinoma, Amino. Acids 40 (2011) 1003–1013.

[51] A.E. Kudinov, J. Karanicolas, E.A. Golemis, Y. Boumber, Musashi RNA-binding proteins as cancer drivers and novel therapeutic targets, Clin. Cancer. Res 23 (2017) 2143–2153.
[52] Miceli F, Soldovieri MV, Weckhuysen S, Cooper EC, Taglialatela M (1993). *KCNQ3-Related disorders*. Adam MP, Feldman J, Mirzaa GM, Pagon RA, Wallace SE and Amemiya A (eds). University of Washington, Seattle Copyright © 1993-2025, University of Washington, Seattle. GeneReviews is a registered trademark of the University of Washington, Seattle. All rights reserved.: Seattle (WA).
[53] F. Cvrčková, R. Ghosh, H. Kočová, Transmembrane formins as active cargoes of membrane trafficking, J. Exp. Bot 75 (2024) 3668–3684.
[54] H. Wang, J.M. Li, W. Wei, R. Yang, D. Chen, X.D. Ma, G.M. Jiang, B.L. Wang, Regulation of ATP-binding cassette subfamily B member 1 by Snail contributes to chemoresistance in colorectal cancer, Cancer. Sci 111 (2020) 84–97.
[55] P. Rappu, Antti M Salo, J. Myllyharju, J. Heino, Role of prolyl hydroxylation in the molecular interactions of collagens, Essays. Biochem. 63 (2019) 325–335.
[56] C. Zhang, B.Z. Wu, K.L. Thu, Targeting kinesins for therapeutic exploitation of chromosomal instability in lung cancer, Cancers 17 (2025) 685.
[57] J.S. Scott, L-E Quek, A.J. Hoy, J.V. Swinnen, Z.D. Nassar, L.M. Butler, Fatty acid elongation regulates mitochondrial β-oxidation and cell viability in prostate cancer by controlling malonyl-CoA levels, Biochem. Biophys. Res. Commun. 691 (2024) 149273.
[58] A.H. Zahalka, P.S. Frenette, Nerves in cancer, Nat. Rev. Cancer 20 (2020) 143–157.
[59] P. Fernandez-Nogueira, A. Noguera-Castells, G. Fuster, L. Recalde-Percaz, N. Moragas, A. Lopez-Plana, E. Enreig, P. Jauregui, N. Carbo, V. Almendro, et al., Histamine receptor 1 inhibition enhances antitumor therapeutic responses through extracellular signal-regulated kinase (ERK) activation in breast cancer, Cancer. Lett 424 (2018) 70–83.
[60] P. Nasarre, R.M. Gemmill, V.A. Potiron, J. Roche, X. Lu, A.E. Baron, C. Korch, E. Garrett-Mayer, A. Lagana, P.H. Howe, et al., Neuropilin-2 is upregulated in lung cancer cells during TGF-beta1-induced epithelial-mesenchymal transition, Cancer. Res 73 (2013) 7111–7121.
[61] W.F. Moriarty, E. Kim, S.A. Gerber, H. Hammers, R.M. Alani, Neuropilin-2 promotes melanoma growth and progression in vivo, Melanoma. Res 26 (2016) 321–328.
[62] C. Grandclement, J.R. Pallandre, Degano S Valmary, E. Viel, A. Bouard, J. Balland, J.P. Remy-Martin, B. Simon, A. Rouleau, W. Boireau, et al., Neuropilin-2 expression promotes TGF-beta1-mediated epithelial to mesenchymal transition in colorectal cancer cells, PLoS. One 6 (2011) e20444.
[63] T.M. Fung, K.Y. Ng, M. Tong, J.N. Chen, S. Chai, K.T. Chan, S. Law, N.P. Lee, M. Y. Choi, B. Li, et al., Neuropilin-2 promotes tumourigenicity and metastasis in oesophageal squamous cell carcinoma through ERK-MAPK-ETV4-MMP-E-cadherin deregulation, J. Pathol 239 (2016) 309–319.
[64] L. Li, X. Jiang, Q. Zhang, X. Dong, Y. Gao, Y. He, H. Qiao, F. Xie, X. Xie, X. Sun, Neuropilin-1 is associated with clinicopathology of gastric cancer and contributes to cell proliferation and migration as multifunctional co-receptors, J. Exp. Clin. Cancer. Res 35 (2016) 16.
[65] T. Lv, X. Wu, L. Sun, Q. Hu, Y. Wan, L. Wang, Z. Zhao, X. Tu, Z.J. Xiao, p53-R273H upregulates neuropilin-2 to promote cell mobility and tumor metastasis, Cell. Death. Dis 8 (2017) e2995.
[66] J.S. Di Martino, A.R. Nobre, C. Mondal, I. Taha, E.F. Farias, E.J. Fertig, A. Naba, J. A. Aguirre-Ghiso, J.J. Bravo-Cordero, A tumor-derived type III collagen-rich ECM niche regulates tumor cell dormancy, Nat. cancer 3 (2022) 90–107.
[67] X. Xie, G. Urabe, L. Marcho, C. Williams, L.W. Guo, K.C. Kent, Smad3 Regulates neuropilin 2 transcription by binding to its 5′ Untranslated region, J. Am. Heart. Assoc 9 (2020) e015487.
[68] T. Kitamura, B.Z. Qian, D. Soong, L. Cassetta, R. Noy, G. Sugano, Y. Kato, J. Li, J. W. Pollard, CCL2-induced chemokine cascade promotes breast cancer metastasis by enhancing retention of metastasis-associated macrophages, J. Exp. Med 212 (2015) 1043–1059.
[69] B. Qian, Y. Deng, J.H. Im, R.J. Muschel, Y. Zou, J. Li, R.A. Lang, J.W. Pollard, A distinct macrophage population mediates metastatic breast cancer cell extravasation, establishment and growth, PLoS. One 4 (2009) e6562.
[70] L.E. Barney, C.L. Hall, A.D. Schwartz, A.N. Parks, C. Sparages, S. Galarza, M. O. Platt, A.M. Mercurio, S.R. Peyton, Tumor cell-organized fibronectin maintenance of a dormant breast cancer population, Sci. Adv 6 (2020) eaaz4157.
[71] L. Dai, M. Li, W.L. Zhang, Y.J. Tang, Y.L. Tang, X.H. Liang, Fibroblasts in cancer dormancy: foe or friend? Cancer. Cell. Int 21 (2021) 184.
[72] M.E. Fane, Y. Chhabra, G.M. Alicea, D.A. Maranto, S.M. Douglass, M.R. Webster, V. W. Rebecca, G.E. Marino, F. Almeida, B.L. Ecker, et al., Stromal changes in the aged lung induce an emergence from melanoma dormancy, Nature 606 (2022) 396–405.
[73] A. Akhmetshina, K. Palumbo, C. Dees, C. Bergmann, P. Venalis, P. Zerr, A. Horn, T. Kireva, C. Beyer, J. Zwerina, et al., Activation of canonical Wnt signalling is required for TGF-beta-mediated fibrosis, Nat. Commun 3 (2012) 735.
[74] T. Ji, Y. Guo, K. Kim, P. McQueen, S. Ghaffar, A. Christ, C. Lin, R. Eskander, X. Zi, B.H. Hoang, Neuropilin-2 expression is inhibited by secreted Wnt antagonists and its down-regulation is associated with reduced tumor growth and metastasis in osteosarcoma, Mol. Cancer 14 (2015) 86.
[75] G.B. Jang, J.Y. Kim, S.D. Cho, K.S. Park, J.Y. Jung, H.Y. Lee, I.S. Hong, J.S. Nam, Blockade of wnt/beta-catenin signaling suppresses breast cancer metastasis by inhibiting CSC-like phenotype, Sci. Rep 5 (2015) 12465.
[76] Y. Kang, Y. Zhang, Y. Zhang, Y. Sun, NRP2, a potential biomarker for oral squamous cell carcinoma, Am. J. Transl. Res 13 (2021) 8938–8951.
[77] M. Caunt, J. Mak, W.C. Liang, S. Stawicki, Q. Pan, R.K. Tong, J. Kowalski, C. Ho, H. B. Reslan, J. Ross, et al., Blocking neuropilin-2 function inhibits tumor cell metastasis, Cancer. Cell 13 (2008) 331–342.